# COMPUTATIONAL FLUID DYNAMICS MODEL OF MULTI-ZONE SINGLE-STRING COMPLETION

By

Nicholas E. Sanders

# Abstract

There are many different ways of running a completion in a well including barefoot openhole completion, single string completions, plug and perf frac completions, submersible pump completions, and multiple string completions. Each of these completions types has its advantages and disadvantages and it is up to the completions engineer to determine what will work best for a given reservoir. When an older well is producing from multiple reservoirs, it is possible that one of the zones would need to produce less so that the well is still economically viable.

This work looks at two common completion designs to model flow from a reservoir into a tubing string. A multi-zone single-string completion is looked at to see how the changing of tubing size and different valve sizes affect the flow from both reservoirs. A single mandrel-valve system is examined for three common sized tubing of 2.875, 3.5 and 4.5 inches being observed. The reservoir produces through a valve of four different sizes, 0.5, 0.375, 0.25, and 0.125 inches. A fourth case is considered looking at a sliding sleeve model with four openings from the tubing to the annular area of 0.125 inches.

These models are run through computation fluid dynamics software to determine flow rates from both the upper and lower reservoir for each of the cases. Pressure gradients and drawdowns of the tubing and reservoir are examined to look at the effects from the different sized tubing and valve combinations. The velocity profiles are also examined to determine if there are any adverse effects from smaller valves compared to larger valves. A comparison is then done between the single valve models and the sliding sleeve model to observe the possible difference between one fluid entry point and four fluid entry points into the tubing.

# Table of Contents

# List of Figures

# List of Tables

# Acknowledgements

# 1 Chapter One: Introduction

## 1.1 Overview

Before a well can be put on production a completion needs to be run. These completions vary wildly from one well to the next and are based on the flow mechanics in the well and the type of fluid or gas being produced. In the case where multiple zones are to be completed in a single well, one approach to this is a single-string multi-zone completion. In this type of completion there is a single string of tubing run in the well, with multiple zones separated by packers.

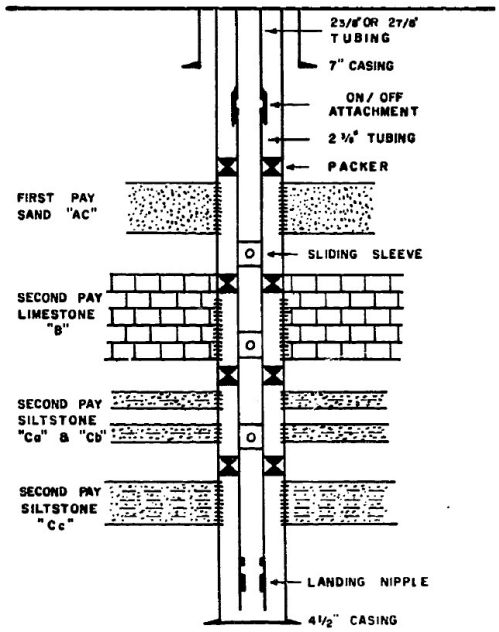


**Figure 1.1 Single-String Multi-Zone Completion**

Single-string multi-zone completions have been successfully used in many areas of the world for a long time. In 1967 the Bahrain field switched from a single or dual completion type to a single-string multi-zone completion to produce from two to four zones in one well bore. This has allowed for lower drilling cost for new wells and lower operating costs by allowing higher GOR oils to help lift the weaker zones (Amear & Almoayyed, 1979). Between 1979 and 1981 Arco started drilling the Kuparuk oil field in Alaska and employed a single-string multi-zone completion technique to produce from their two different zones (Jensen et al., 2012).

With this type of completion, the lowest zone would be produced into the casing and up the bottom of the tubing while all other zones are produced through a sliding sleeve or production mandrel setup. This setup allows for selectively producing zones based on a predefined plan for production.

Production mandrels are the preferred method for production form the area between the packers as they are more controllable in the size of the flow area provided for the fluid.

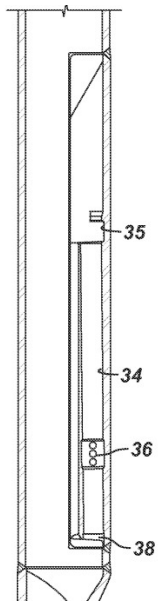


**Figure 1.2 Mandrel Body (Rae, 2013)**

Figure 1.2 shows a typical mandrel, #36 in the figure shows the area where the fluid flows from the annulus to the well bore. Figure 1.3 shows the mandrel with a valve inserted. Essentially the fluid flows though the ports (#36 in Figure 1.2) and into the port on the valve (#46 on Figure 1.3). From there the fluid flows through the valve and out the top into the tubing of the wellbore. These valves can have different port sizes and can act as a choke for the fluid coming in from the annulus.

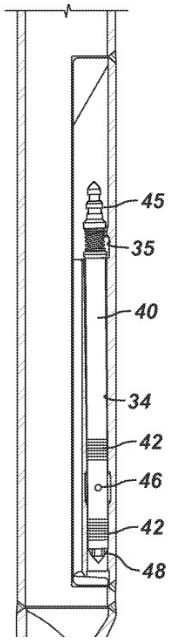


**Figure 1.3 Mandrel Valve (Rae, 2013)**

The sliding sleeve completions is not as common for single-string multi-zone setups, but have been used in some areas for production. These sleeves are commonly used in frac completions to allow for isolation of zones during frac operations and can be used later in the well's life to close off areas that are not producing as desired. In the single-string multi-zone completion setup, the sleeves are used to allow flow from the annulus area into the wellbore.

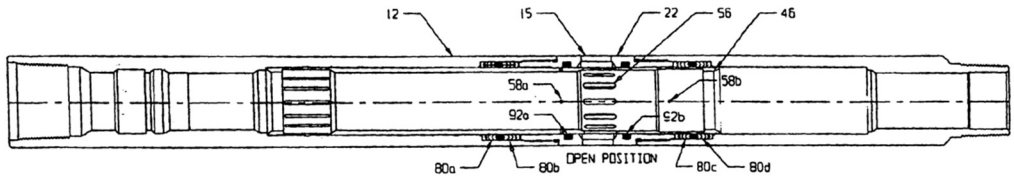


**Figure 1.4 Open Sliding Sleeve (Kaszuba, 2004)**

Figure 1.4 shows a sliding sleeve in the open position where #56 in the image shows the flow ports, which can also be sized as a choke but in general allow for more flow due to the larger size and number of ports. Figure 1.5 shows a sliding sleeve in the closed position. These sleeves have an internal section that moves up and down to allow flow through the opening in the sides between the annulus and the wellbore and can open either upward or downward depending on their design.

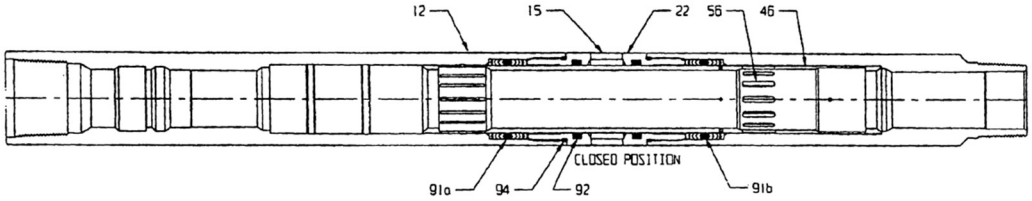


**Figure 1.5 Sliding Sleeve Closed (Kaszuba, 2004)**

These types of completion can be used in gas wells or oil wells, on producers or injectors. When one zone is not producing as it should, are there ways to change that? Usually a well intervention is planned to look into how a well is producing or injecting. These interventions can be costly and can result in undesired changes or downtime for the well. Using computation fluid dynamics, it is possible to model the well completion and the surrounding reservoir, to see how the well will respond to different changes. This approach requires large amounts of computer time but many different scenarios can be looked at while the well is still online and the best approach can be picked based on analytical results. The well intervention is still needed to make the changes but the modeling can take the guess work out of what would be the best route to take.

## 1.2 Objective

The objective of this work is to create small models of a single-string multi-zone completion and the surrounding wellbore to determine if it is feasible to use computation fluid dynamics to determine if changes in the wellbore completion will produce the desired changes in the production. Using the academic version ANSYS Fluent, a small base model will be made to show that the Fluent program matches with established IPR equations. After this, the model will be modified to show three different tubing sizes with four different valve size cases each to determine the best setup for producing the reservoir. A model with a sliding sleeve setup will also be built and compared to the three models with a mandrel-valve type setup. These models will use liquid oil as the single phase fluid. Comparison of the flow rates, pressure drawdown of the reservoir, and velocity profiles were be performed to help with the determinations of which setup is best for production.

# 2 Chapter Two: Literature Review

## 2.1 CFD in the Petroleum Industry

Computational fluid dynamics CFD has found its way into the petroleum industry over the last decade in various different aspects. Longfellow et al. used CFD to model a plunger lift system in a horizontal well (Longfellow & Green, 2014). This work showed that the CFD model was within 8% for observed fall rates for plunger lift systems. It also looked at different types of plungers to determine if one was more appropriate for a given application, as well as looking at modeling some of the issues of plungers in horizontal wells including uneven wear and gas blow-by. Longfellow et al. also showed that along with the positives CFD encountered issues with working in unsteady multi-phased flow environments present in the horizontal tubing.

Zhou et al. used CFD to model flow inside of coiled tubing (Zhou & Shah, 2003). This work looked at both Newtonian and non-Newtonian fluids inside of coiled tubing. Largely concerned with the flow due to the curvature of the coil on the reel the results compared well with previous theoretical and numerical studies. Newtonian fluids showed that in laminar flow the velocity profile in the curved tubing was more distinct than the parabolic one seen in straight tubing. In contrast the turbulent flow in curved tubing and straight tubing showed similar velocity profiles. THE CFD modeling showed that as Reynolds numbers increased the secondary flow, components of the flow that are significantly different in both velocity and direction from what is predicted, were confined to a thin boundary layer. Lastly, the friction pressure from the turbulent Newtonian fluid experiments performed on coiled tubing reels and the CFD agreed well.

Li et al. used CFD to model the flow characteristics around a subsurface safety valve SSSV (Li, Zhang, Davis, & Hamid, 2005). SSSV's are used in a wellbore to close during an uncontrolled release on surface. The pressure gradient across the valve will drop in an uncontrolled release and the valve will close due to this difference, sealing off the wellbore below from the surface. This work is concerned with the possibility that high rate gas flow will prevent the SSSV from closure. The combination of CFD models and full scale physical tests has shown comparable results at different flow rates and under different flow conditions for which the valve was designed to work.

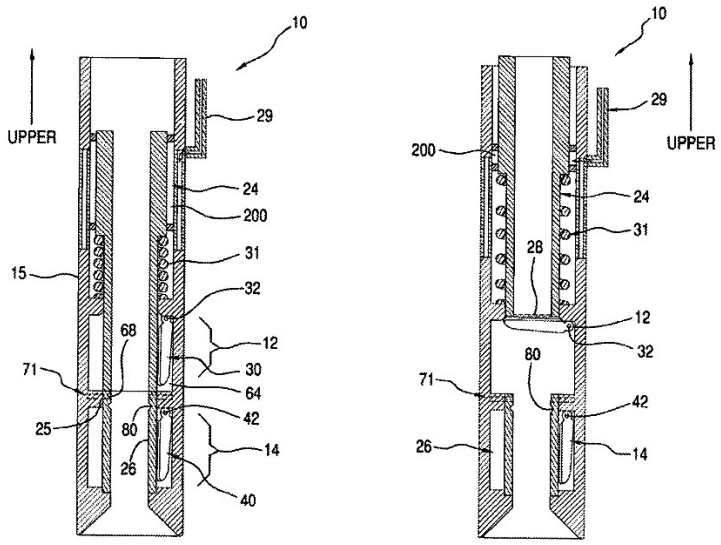


**Figure 2.1 SSSV Showing Flapper Valve Open and Closed (Reaux, 2013)**

## 2.2 CFD and Reservoir Inflow

CFD has not been used only to model flow around plunger lift systems or SSSV's but also to model inflow performance from a wellbore. Byrne et al. looked at how close CFD models were to actual inflow performance from laboratory studies on core samples (M. Byrne, Alejandra, & Chavez, 2009). This was the first time that CFD was used to predict well performance based on high quality laboratory testing. The authors combined laboratory testing to determine permeability for different zones from the undamaged reservoir to the invaded zone and out through the mud cake to the wellbore. These models showed that impacts from the mud were not significant for any of the tests performed and required a reduction in the formation permeability of 95% before significant reduction in the flow rate was seen. This study has allowed for CFD to be used in the design of drilling systems during the well planning stages.

Jimenez et al. used CFD to model the inflow of single and multiple fractured wells in their study from 2009 (Jimenez & Chavez, 2009). Their work showed that CFD was a practical engineering tool that provided core information and enhances decision making processes for completions. They used CFD to simulate two different case studies, one a vertical well and the second, a deviated well. The first study showed a reservoir with five different layers of varying permeability.

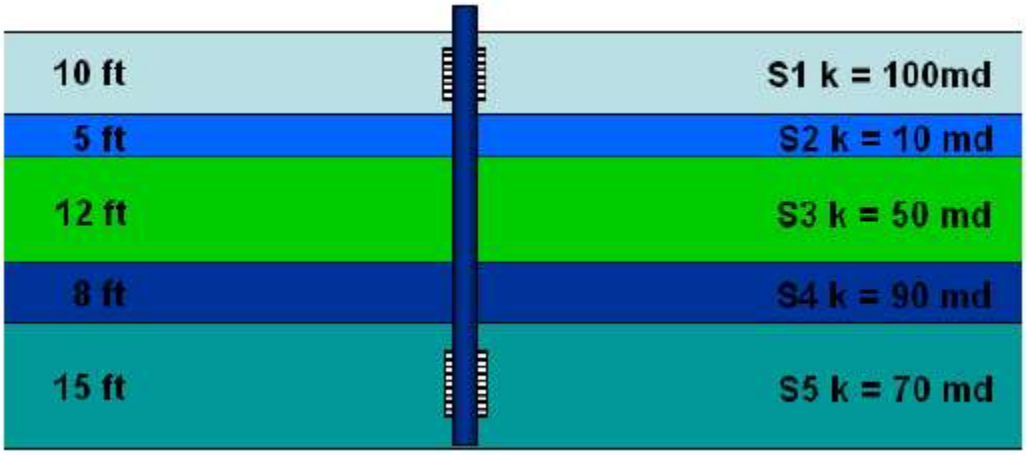


**Figure 2.2 Vertical Well Setup (Jimenez & Chavez, 2009).**

The completion was planned in three phases; first, the middle layer, S3, was perforated and then fractured. The third stage was perforating the upper and lower layers, S1 and S5 respectively, and it was assumed that there was no interaction between the fractures and the perforation. This model showed that an increase of 60% was seen in the S3 zone when fractured over just perforations. The second model was a deviated well through the same reservoir setup.

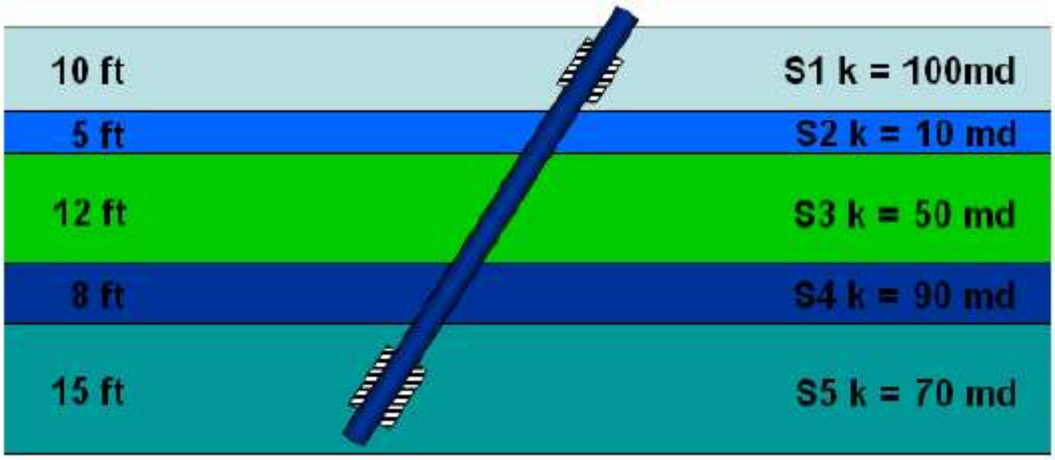


**Figure 2.3 Deviated Well Setup (Jimenez & Chavez, 2009).**

This completion was done with similar steps to the vertical well model, perforating and fracturing S4, perforating and fracturing S2, and finally perforating S1 and S5 again the same as in the vertical model. This setup resulted in a reduction of production from the S3 layer over the same setup in the vertical model. The possibility of creating communication with a water zone during fracturing in S4 dictated that only S2 was fractured. This showed a 20% to 30% decrease in total production from the vertical model with a fracture in S3.

Byrne et al. produced a paper on modeling inflow with CFD in 2010 (M. T. Byrne, Jimenez, Rojas, & Chavez, 2010). This time they looked at fluid flow into a horizontal wellbore considering the invaded zone and mud cake again. The first model looked at the production from a horizontal well with formation damage due to invaded zone and a mud cake inside the wellbore. Different flowing pressures were assigned to different zones in the well to better represent the drawdown of the well.

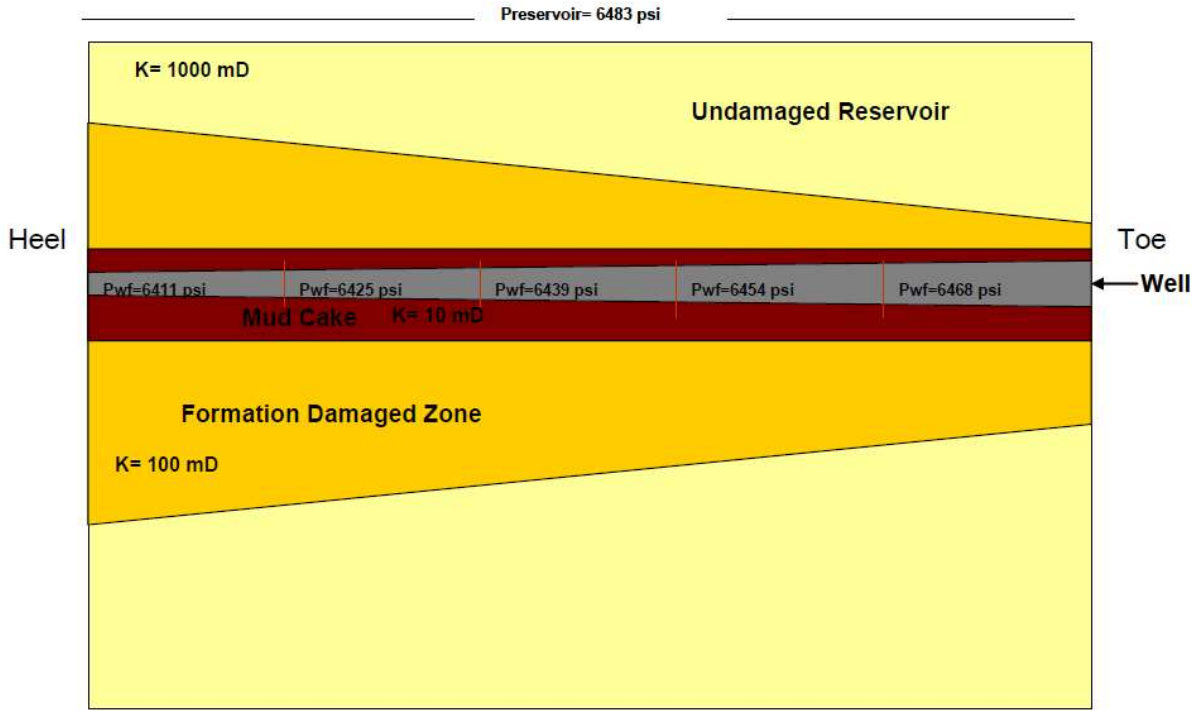


**Figure 2.4 Setup for Case 1 (M. T. Byrne et al., 2010)**

This model showed that the velocity profile of the well has the highest velocity on the high side of the heel section of the well. A second model was run showing an open horizontal well without an invaded zone or mud cake, this model also did not have the different pressure drawdown zones preset. This model showed higher production at the heel zone than the model with mud cake as one would expect. The pressure drawdown in the second model was consistent from heel to toe of the well whereas, due to the mud cake and invaded zone, the first model had higher drawdown shown in the mass flow contours.

A comparison of skin factors for perforated completions was performed by Sun et al in 2013 (Sun, Li, Gladkikh, Satti, & Evens, 2013). A CFD model to compare skin factors between the CFD skin factor and the Karakas and Tariq model from 1991 was performed. The Karakas and Tariq model shows substantually less skin factor then the CFD model under both crushed zone, the area of crushed rock surrounding the perforation tunnel, and permeability anisotropy. However if the crushed zone is considered with isotropic permeability and the permeability damage ratio $K_c/K_H$ is assumed with the maximum original permeability $K_H$ in the denominator, the CFD simulations and the Karakas and Tariq

model are in agreement. This highlights the need for further study in the area of anisotropy in the crushed zone. Under other cases with an isotropic formation with no damage the CFD model and the Karakas and Tariq model compare well with the CFD skin factor usually being higher. The only other area where these two models did not compare is in the case of no crushed zone in the tip of the perforation.

Theppornprapakorn wrote his thesis in 2013 on a CFD comparison between openhole sleeve completions and plug and perf completions in a hydraulic fractured horizontal well (Theppornprapakorn, 2013). This work used a horizontal well and gas as the fluid but started with a validation model using water as an incompressible fluid to prove the model. This validation model used a reservoir model shown in Figure 2.5 that had a horizontal well with a drainage radius of 300 feet and using a symmetry plane to only need to model half of the reservoir.

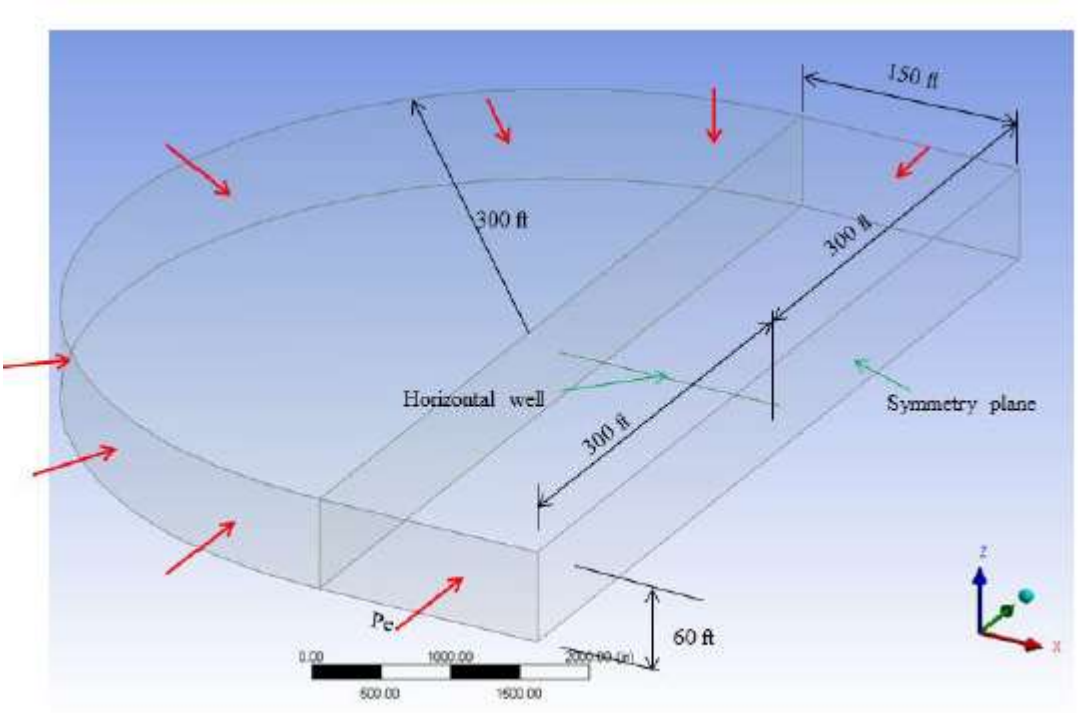


**Figure 2.5 General Model Setup (Theppornprapakorn, 2013)**

The validation model compared almost exactly with the IPR curve, within 0.2%. The validation model was then run using gas as the fluid, a mixture of $CH_4$ and $C_2H_6$. This model resulted in the CFD model producing slightly higher results, as much as 4.9% at lower drawdown pressure, than the IPR curve.

The model was then run with a single transverse fracture intersecting the plug in perf P-n-P completion. This model was performed with two perforations 180 degrees apart from each other reaching 9 inches into the reservoir. Where there are no perforations the well is considered closed off to the reservoir. These perforations connect to a fracture body at their tip as is shown in Figure 2.6.

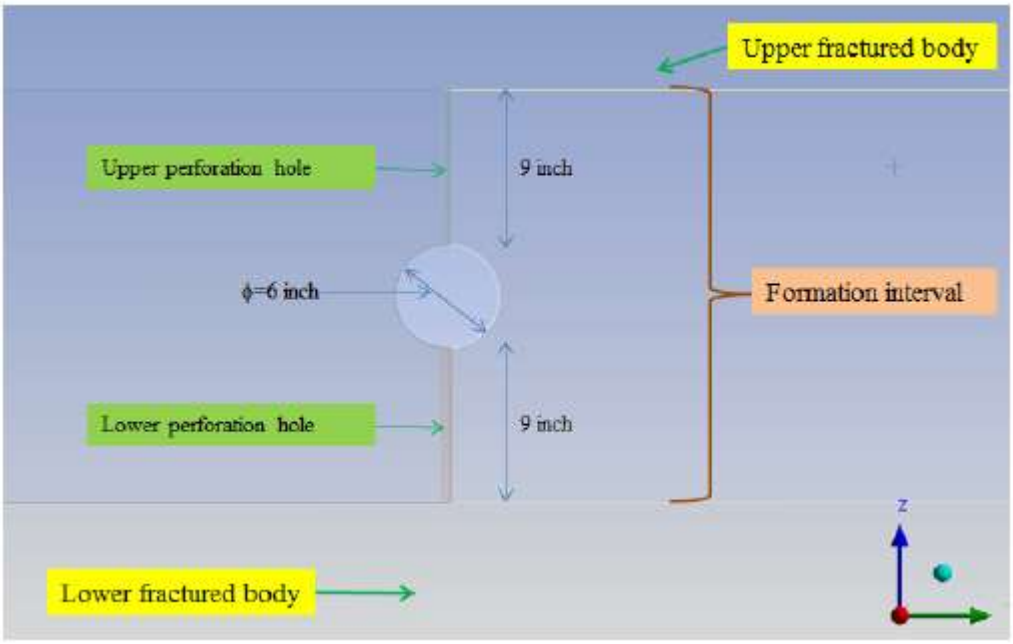


**Figure 2.6 P-n-P Setup (Theppornprapakorn, 2013)**

This model was run with a base case using different fracture conductivities (15,000; 13,000; 11,000; 9,000;7,000; 5,000; 3,000;, 1,000; and 500 md-ft) using a fracture half-length of 150 ft and a flowing bottom hole pressure of 1000 psi. Three different cases were then examined and compared to the base case. These three cases were changing the fracture width from the base case on 0.01 inches to 0.1 or 0.3 inches, changing the penetration ration of the fracture from 150 feet to 200 feet and 250 feet, and changing the vertical to horizontal permeability ratio from the base case of 0.1 to 0.5 and 1.0.

The openhole multistage completion model (OHMS) was designed in much the same way as the P-n-P model. This model differed in the fact that there are no perforations and the entire well is considered open to the wellbore. The fractures were connected to the wellbore down the full length of the well. This setup was then subjected to the same base model conditions and the same three cases as the P-n-P model.

The results show that for all the cases the OHMS produced at a higher rate than the p-n-p completion as would be expected. For the first case study models showed that for larger fracture propped width the flow rate was higher although not much change was seen for each step. For the second case study the deeper the penetration of the fracture, correlated to a much larger increase in production from the reservoir for both the P-n-P and OHMS completions. This again is to be expected because as the fractures run deeper into the reservoir the production will be higher because more of the reservoir is able to flow to the much more permeable area inside the fracture. The third case showed the difference in the permeability ratio ($k_v/k_h$). This showed for both the P-n-P and OHMS model that the lower the $k_v/k_h$

values the higher the production. This will shower a larger effect on thicker reservoirs over thinner reservoirs.

In 2015 Molina wrote a thesis on the application of computation fluid dynamics to the near-wellbore modeling of a gas well (Molina, 2015). This thesis used CFD to look at the difference between a gravel pack completion and a frac-pack completion. A verification case was the first case run just as was in the Theppornprapakorn thesis. This case was built as a round reservoir with radius of 3.5 feet, a wellbore radius of 0.125 feet, a height of 2 feet, viscosity of 0.89 cP, and permeability of250 mD. These values were plugged into Equation 2.1 and resulted in the values presented in Table 2.1.

$$q = 0.00708\left(\frac{kh}{\mu}\right)\frac{\Delta P}{\ln\left(\frac{r_e}{r_w}\right)} \quad \textbf{[2.1]}$$

Also present in Table 2.1 are the values that were calculated by Fluent and the relative error. It can be seen that the Fluent program does a good job approximating the flow for the validation model.

| Radial Distance (ft) | Predicted P(r) (psig) | Analytical P(r) (psig) | Relative Error (%) |
|---|---|---|---|
| 0.125 | 800.36 | 800.00 | 0.05 |
| 0.263 | 889.15 | 888.58 | 0.06 |
| 0.538 | 975.34 | 974.09 | 0.13 |
| 0.745 | 1,014.37 | 1,012.84 | 0.15 |
| 1.020 | 1,052.24 | 1,050.36 | 0.18 |
| 1.227 | 1,074.26 | 1,072.35 | 0.19 |
| 1.503 | 1,098.62 | 1,096.50 | 0.20 |
| 1.778 | 1,118.85 | 1,116.58 | 0.22 |
| 2.054 | 1,136.20 | 1,133.76 | 0.22 |
| 2.260 | 1,147.76 | 1,145.19 | 0.22 |
| 2.536 | 1,161.46 | 1,158.90 | 0.22 |
| 2.742 | 1,170.87 | 1,168.24 | 0.22 |
| 3.018 | 1,182.31 | 1,176.66 | 0.22 |
| 3.224 | 1,190.21 | 1,187.56 | 0.22 |
| 3.500 | 1,200.03 | 1,197.33 | 0.23 |

**Table 2.1 Validation Model Results (Molina, 2015)**

At this point two simulations were set up, one for the gravel pack and one for the frac-pack completion. Figure 2.7 show the gravel pack completion.

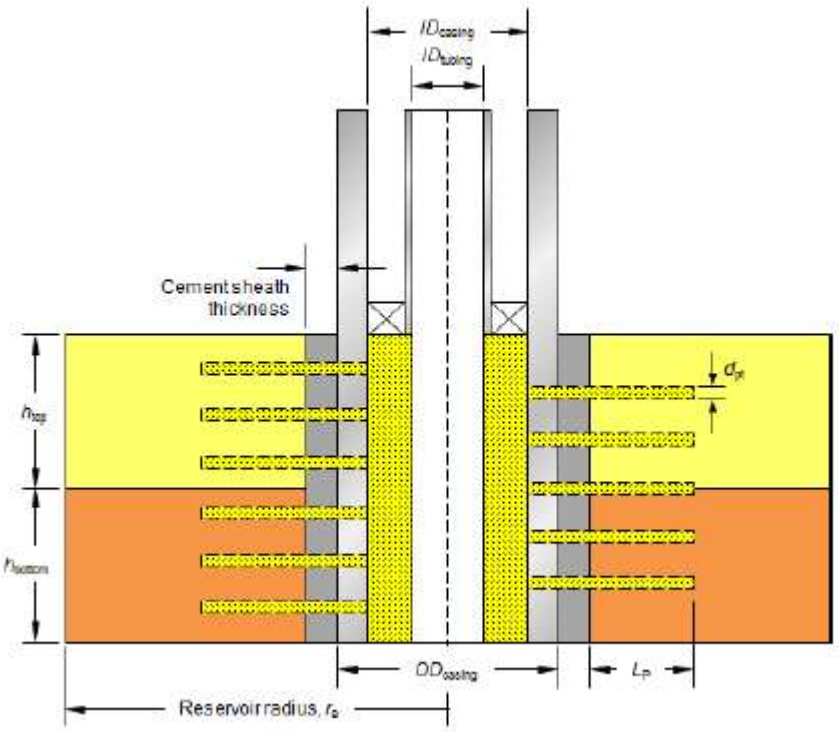


**Figure 2.7 Gravel Pack Setup (Molina, 2015)**

The values used for the model are shown in Table 2.2.

| | | | |
|---|---|---|---|
| Top layer height | $h_{top}$ | 1 | ft |
| Bottom layer height | $h_{bottom}$ | 1 | ft |
| External reservoir radius | $r_e$ | 3.5 | ft |
| Wellbore radius | $r_w$ | 0.5 | ft |
| Production casing ID | $d_i$ | 6 | in |
| production casing OD | $d_o$ | 6 5/8 | in |
| cement sheath thickness | -- | 1 3/16 | in |
| Production tubing string ID | -- | 3 | in |

**Table 2.2 Near-Wellbore Geometry Dimensions (Molina, 2015)**

These models were set up to run a series of tests starting with the gravel pack completion. The length of the perforations was varied in the gravel pack completion to determine the best length for optimal production from the two layer reservoir. The first case was set up with perforations 0.5 feet in length into the reservoir and the second case being perforations with a length of 1.0 feet into the reservoir. Between these two setups the case with a perforation length on 1.0 feet produced more than the case with a perforation length of 0.5 feet. Molina showed the pressure drawdowns for each of these cases and the

flow patterns for flow from the reservoir into the perforations. Figure 2.8 shows the flow patterns going more into the tip of the perforations than any other part.

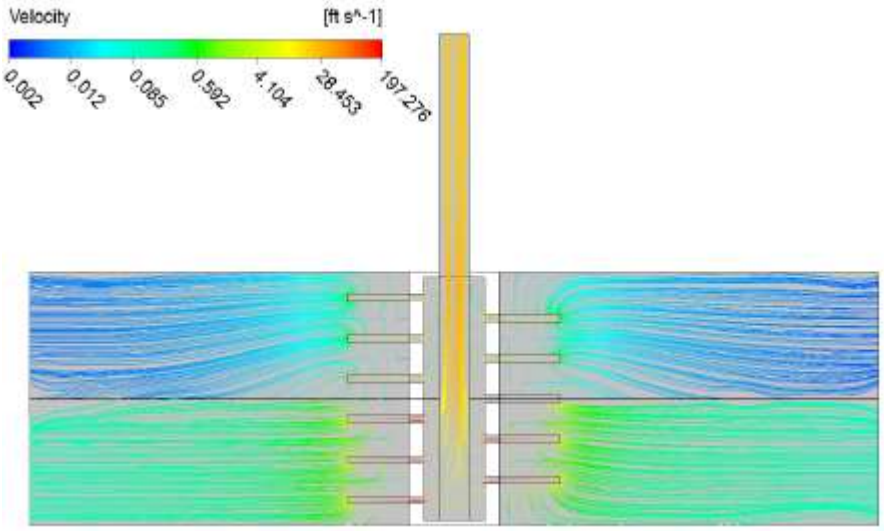


**Figure 2.8 Cross-sectional flow pattern (Molina, 2015)**

The frac-pack completion setup is similar to the gravel pack completion and is shown in Figure 2.9.

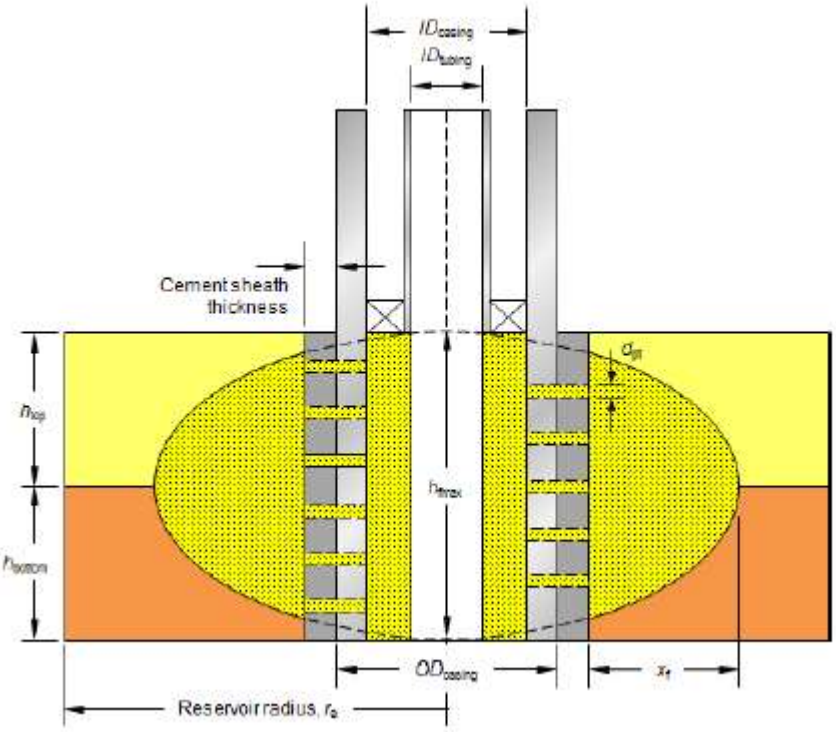


**Figure 2.9 Frac-Pack Setup (Molina, 2015)**

This case was different than the gravel pack completion due to the bi-wing fracture that was modeled emanating from the perforations. The frac-pack completion showed a 73.56% and 52.58% increase in production over the two case studies for the gravel pack completion.

$$\frac{\partial p}{\partial x} = -\frac{u}{k} q \qquad \textbf{[2.2]}$$

In 1901 Phillip Forchheimer was working with Darcy's equation (Equation 2.2) and noticed that for substantially high Reynolds numbers in the porous media, Darcy's equation did not work. He was able to develop a term for the inertial effects and applied it to Darcy's equation creating Equation 2.3.

$$\frac{\partial p}{\partial x} = -\frac{u}{k} q - \beta \rho q^2 \qquad \textbf{[2.3]}$$

The frac-pack model was first run with a value of $\beta = 0$ and showed that at high flow rates there could be as much as a 96.65% overestimation of gas production. The model was then run with a $\beta > 0$ value and produced values closer to the expected values from the equations. Again pressure drawdown plots were presented for each drawdown pressure.

# 3 Chapter Three: Computational Fluid Dynamics Overview

## 3.1 Introduction to Computational Fluid Dynamics

Fluid dynamics started in the seventeen hundreds with the creation of experimental techniques and progressed in the eighteenth and nineteenth centuries with more theoretical aspects. Until the mid-twentieth century experimental and theoretical techniques were the two components that made up fluid dynamics, however, with the computer revolution came a new third dimension in computational fluid dynamics CFD (Anderson, 1995). CFD has become common place in many industries from aerospace and automotive to biomedical engineering and electrical and electronics engineering. CFD uses the fact that fluid flows are always controlled by three aspects, conservation of mass, Newton's second law, and conservation of energy. These three equations, in their original form are either partial differential equations or integral equations and CFD is used to replace these equations with discrete algebraic equations (Anderson, 1995).

Generally, CFD problems can be separated into three aspects for solving the problem: pre-processing, solver, and post-processing. In the pre-processing stage a model is designed based on the desired problem to solve. This will include building a geometrical model, generating the grid, selection of the physical process to be modeled, fluid property definition, and boundary condition selection. In the solver section of the process the integration of all the governing equations is performed over the control volumes, discretization is performed, and the algebraic equations are solved in an iterative process. Finally in the post-processing stage the domain geometry and grid is displayed, vector plots can be made along with 2D and 3D plots. This step is used to display the final solution to the problem and interoperate the results from the algebraic equations (Versteeg & Malalasekera, 2007).

The pre-processor step is used to define the problem. A CAD model, in either 2D or 3D, is built to describe the problem. This CAD model is then sent through a meshing program to divide the model up into a finite number of nodes. Each of these nodes will have the governing equations solved specifically for it, thus the larger number of nodes the longer the processing time on finding a solution to the problem. The meshing nodes are generally not all the same since as there will be large areas to cover and smaller areas that require more detail. Generally the fluid properties are known for the problem being posed, air is used if it is an aerodynamic problem or other fluids based on the type of model being proposed, water for shipping hydraulic models, or as in this thesis oil is used with a known density and viscosity. Over half the time of building the CFD model will be spent in defining these steps as the more effort that is put into the geometry design process and the meshing, the less troubleshooting later when running the model.

The solver step will require the most processing time and power as this is where the actual calculations will be performed. Each node will have the governing equations solved for it during each of

the iterations until a convergence criterion is met. These problems can be solved on either a pressure based or density based setup. The pressure based solver uses an algorithm which belongs to a general class of methods called the projection method (Chorin, 1968). In this method the pressure equation is derived from the continuity and momentum equations in a way that the velocity field satisfies continuity. There are two different types of pressure based solvers, segregated algorithm and coupled algorithm. The pressure based segregated algorithm, used in this work, uses an algorithm where governing equations are solved segmentally. The pressure based-coupled algorithm solves a coupled system of equations including the momentum and pressure-based continuity equations. This coupled algorithm uses 1.5-2 times the computer memory as the segregated algorithm but converges at a much faster rate. Figure 3.1 shows a flow chart for these two different pressure-based algorithms. The density based solver solves the continuity, momentum, energy, and species equations simultaneously much like the coupled pressure-based solver (ANSYS, 2013b).

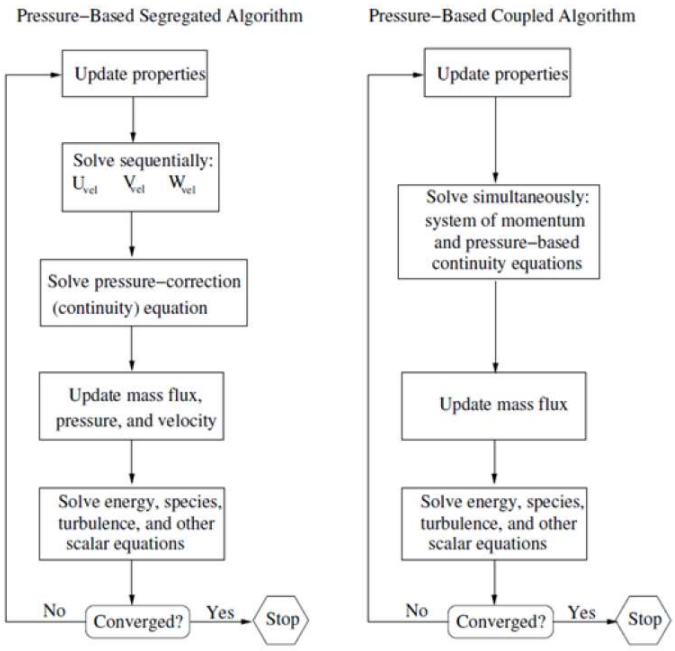


**Figure 3.1 Pressure-Based Solver Algorithms (ANSYS, 2013b)**

Post-processing is the step in which the solution is examined and different 2D and 3D diagrams can be produced. In this step the results are analyzed to make sure they fit the criteria set aside for proper solving of the problem. With the advancement of computers in recent years, these results have started to include animations of the flowline from the results.

## 3.2 Computational Fluid Dynamics Governing Equations

The solver step of the process sets out to solve a system of equations that include the momentum and mass equations. As was stated previously the three aspects that control fluid flow are the

conservation of mass, Newton's second law, and the conservation of energy. Since the question being posed in this thesis is an incompressible fluid and the system is isothermic, the conservation of energy can be ignored. This leaves the conservation of mass and Newton's second law that need solved for each node in the system.

The conservation of mass is a simple concept, mass is neither created nor destroyed in the system. In this case this means that the same amount of fluid that comes into the reservoir at the outer boundary exits the system at the outlet of the casing.

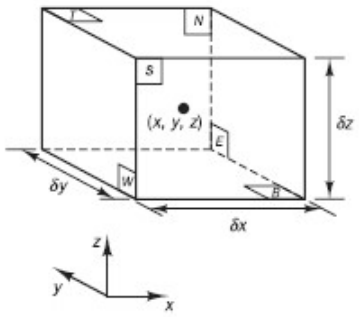


**Figure 3.2 Fluid Element for Conservation Laws (Versteeg & Malalasekera, 2007)**

Figure 3.2 shows a single node for model with sides δx, δy, and δz. This node will be used to derive the conservation of mass and momentum equation that will be used by the solver. Since conservation of mass states that mass in equals mass out it can be said that in three dimensions

$$\frac{\partial}{\partial t}(\rho\delta x\delta y\delta z) = \frac{\partial \rho}{\partial t}\delta x\delta y\delta z \qquad [3.1]$$

The mass flow rate across the face of the element can be given, where flow into the box is given a positive sign and flow out of the box is given a negative sign. Figure 3.3 shows the net rate in flow of mass across each interface.

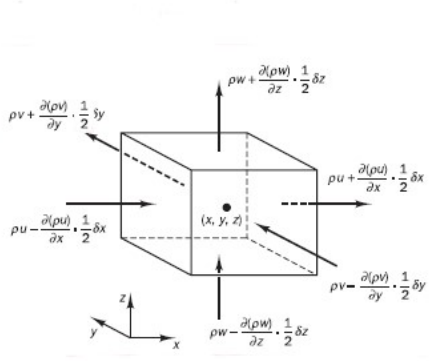


**Figure 3.3 Mass flow in and out of a fluid element (Versteeg & Malalasekera, 2007)**

$$\left(\rho u - \frac{\partial(\rho u)}{\partial x}\frac{1}{2}\partial x\right)\partial y\partial z - \left(\rho u - \frac{\partial(\rho u)}{\partial x}\frac{1}{2}\partial x\right)\partial y\partial z + \left(\rho v - \frac{\partial(\rho v)}{\partial y}\frac{1}{2}\partial y\right)\partial x\partial z - \left(\rho v - \frac{\partial(\rho v)}{\partial y}\frac{1}{2}\partial y\right)\partial x\partial z + \left(\rho w - \frac{\partial(\rho w)}{\partial z}\frac{1}{2}\partial z\right)\partial x\partial y - \left(\rho w - \frac{\partial(\rho w)}{\partial z}\frac{1}{2}\partial z\right)\partial x\partial y \quad \textbf{[3.2]}$$

witch simplifies to

$$\frac{\partial \rho}{\partial t} + \nabla(\rho u) = 0 \quad \textbf{[3.3]}$$

Since the fluid is considered incompressible the density is constant and Equation 3.3 becomes

$$\nabla u = 0 \quad \textbf{[3.4]}$$

Newton's second law states that the force on an object is equal to the object's mass times it's acceleration. In the case of a moving fluid the rate of increase of momentum is equal to the sum of the forces acting on the fluid. Equation 3.5 gives the rate of increase of the x-, y-, and z-momentum per unit volume

$$\rho\frac{Du}{Dt}, \rho\frac{Dv}{Dt}, \rho\frac{Dw}{Dt} \quad \textbf{[3.5]}$$

The total force per unit volume is given by

$$\frac{\partial(-p + \tau_{xx})}{\partial x} + \frac{\tau_{yx}}{\partial y} + \frac{\tau_{zx}}{\partial z} \quad \textbf{[3.6]}$$

Setting Equation 3.5 equal to Equation 3.6 results in the component of momentum equation in the x, y, or z direction respectively

$$\rho\frac{Du}{Dt} = \frac{\partial(-p + \tau_{xx})}{\partial x} + \frac{\tau_{yx}}{\partial y} + \frac{\tau_{zx}}{\partial z} + S_{Mx} \quad \textbf{[3.7a]}$$

$$\rho\frac{Du}{Dt} = \frac{\tau_{xy}}{\partial x} + \frac{\partial\left(-p + \tau_{yy}\right)}{\partial y} + \frac{\tau_{zy}}{\partial z} + S_{My} \quad \textbf{[3.7b]}$$

$$\rho\frac{Du}{Dt} = \frac{\tau_{xz}}{\partial x} + \frac{\tau_{yz}}{\partial y} + \frac{\partial(-p + \tau_{zz})}{\partial z} + S_{Mx} \quad \textbf{[3.7c]}$$

where τ is the stress component. The momentum equation can also be written in the following form

$$\frac{\partial}{\partial y}(\rho \boldsymbol{v}) + \nabla \cdot (\rho \boldsymbol{v}\boldsymbol{v}) = -\nabla p + \nabla \cdot (\tau) + \rho \boldsymbol{g} + \boldsymbol{F} \quad \textbf{[3.8]}$$

where τ is

$$\tau = \mu \left[ (\nabla \boldsymbol{v} + \nabla \boldsymbol{v}^T) - \frac{2}{3} \nabla \cdot \boldsymbol{v} I \right] \quad \textbf{[3.9]}$$

Discretization is the practice of transforming continuous differential equations into discrete difference equations that can be solved numerically. There are three common methods for discretization: finite difference, finite element, and finite volume methods. Of these three methods ANSYS fluent uses the finite volume method. This method is used to divide the problem into a finite number of nodes which is called meshing. The differential equations given above are then integrated over the nodes which results in a unique set of algebraic equations for each node.

ANSYS Fluent has different options for which scheme can be used for the discretization process. Each of these options has different advantages and disadvantages based on the type of problem to be solved. For this work a second-order upwind scheme was chosen, with upwind meaning the face value is derived from quantities upstream of the direction relative to the normal velocity (ANSYS, 2013b).

## 3.3 Turbulence Modeling

### 3.3.1 Laminar and Turbulent Flow

Fluids used in engineering calculations can take one of two forms, laminar or turbulent. Laminar flow is characterized by flow in layers that are adjacent to each other and these layers slide past each other smoothly in an orderly fashion. When Equations 3.7a,b, and c above show the Navier-Stokes equations and combined with the continuity equation (Equation 3.3) can fully describe simple laminar flows. Turbulent flow is cauterized by random chaotic movement of the particles that is hard to describe easily. The random chaotic motion of turbulent flow makes the mathematical description of the flow difficult. Unlike laminar flow, turbulent flow always has a three-dimensional spatial characteristic with rotational eddies dominating the flow.(Versteeg & Malalasekera, 2007)

Flow in pipes is a special case for laminar and turbulent flow and is known as a turbulent flow without a inflection point. Pipe flow is both laminar and turbulent at the same time with the area nearest the wall being laminar and the area in the middle of the pipe being turbulent. Inertial forces dominate the flow further away from the wall with viscous effects dominating at the near wall region. At the wall a very thin layer of fluid known as the linear or viscous sub-layer is stationary. Beyond the viscous layer there is a layer where both viscous and turbulent flows are both important known as the log-law layer.

The next layer out from the pipe is called the viscosity-deflect law layer or the law of the wake. This layer can overlap with the log-law layer but the two layers have to be equal. (Tennekes & Lumley, 1972) These layers are split into two groups, the inner region and the outer region. The inner regions is made up of the linear sub layer, a buffer layer, and the log-law layer and makes up 10-20% of the total thickness. The outer region is made up of the law of the wake layer and is dominated by inertial flows free from viscous effects. (Versteeg & Malalasekera, 2007) For our calculation purposes a Reynolds number of 2100 will be used to differentiate between laminar and turbulent flow.

### 3.3.2 Turbulence Flow Models

Turbulence models can be split into three categories, Reynolds-averaged Navier-Stokes (RANS) equations, large eddy simulations, and direct numerical simulations. A few of the more popular RANS models will be looked at, for more information about large eddy simulations and direct numerical simulations refer to Versteeg et al. (Versteeg & Malalasekera, 2007). The majority of turbulent flow in engineering calculations is done using RANS model. These calculations require a turbulence model to be developed for the Reynolds stress and scalar transport terms as well as close the mean flow equations. The mixing length model, k-ε, and k-ω models will be looked at in more detail.

#### *3.3.2.1 Mixing Length Model*

The mixing length model attempts to describe the stress as a simple algebraic formula for μ. This model has been found to work well for simple two-dimensional turbulent flows, is easy to implement, requires very little computing power, and has good predictions for this shear layers. (Versteeg & Malalasekera, 2007) Some of the disadvantages include it being completely incapable of describing flows with separation ad recirculation and only calculating the mean flow properties and turbulent shear stress.

The kinematic turbulent viscosity is given by Equation 3.10 and the dynamic turbulent viscosity is given by Equation 3.11.

$$v_t = C\vartheta l \quad \textbf{[3.10]}$$

$$\mu_t = C\rho\vartheta l \quad \textbf{[3.11]}$$

where c is a dimensionless constant of proportionality. For simple two-dimensional flows it can be shown that

$$\vartheta = cl\left|\frac{\partial U}{\partial y}\right| \quad \textbf{[3.12]}$$

Combining Equation 3.10 and Equation 3.12 the Prandtl's mixing length model is formed as

$$v_t = l_m^2 \left|\frac{\partial U}{\partial y}\right| \quad \textbf{[3.13]}$$

With the turbulent Reynolds stress described as

$$\tau_{xy} = \tau_{yx} = -\rho\overline{u'v'} = \rho l_m^2 \left|\frac{\partial U}{\partial y}\right| \frac{\partial U}{\partial y} \quad \textbf{[3.14]}$$

The mixing length model is not used itself in many CFD applications but will be combined into other models describing near wall flow.

#### *3.3.2.2 The k-ε Model*

The k-ε model is concerned with the mechanisms the effect kinetic turbulent energy. This model is the most widely used and validated turbulence model. It is used in calculating thin shear layer and recirculating flows in a wide range of industrial applications. The k-ε model is more difficult to implement than the mixing length model in the terms of computing time, and has a hard time predicting rotating flows, flows driven by anisotropy of Reynolds stresses, and flows with large extra strains. (Versteeg & Malalasekera, 2007)

The equations for the k-ε model are given as

$$\frac{\partial(\rho k)}{\partial t} + div(\rho k \boldsymbol{U}) = div\left[\frac{\mu_t}{\sigma_k} grad\ k\right] + 2\mu_t S_{ij} \cdot S_{ij} - \rho\varepsilon \quad \textbf{[3.15]}$$

$$\frac{\partial(\rho \epsilon)}{\partial t} + div(\rho \epsilon \boldsymbol{U}) = div\left[\frac{\mu_t}{\sigma_\epsilon} grad\ \epsilon\right] + C_{1\epsilon}\frac{\epsilon}{k} 2\mu_t S_{ij} \cdot S_{ij} - C_{2\epsilon}\rho\frac{\epsilon^2}{k} \quad \textbf{[3.16]}$$

These equations as described as the rate of change of k or ε plus the transport of k or ε by convection equals the transport of k or ε by diffusion plus the rate of production of k or ε minus the rate of destruction of k or ε. The adjustable constants in the equation are given by $C_\mu = 0.09$, $\sigma_k = 1.00$, $\sigma_\varepsilon = 1.30$, $C_{1\varepsilon} = 1.44$ ad $C_{2\varepsilon} = 1.92$ with the constants arrived at by data fitting of a wide range of turbulent flows.

This work used the realizable k-ε model. The realizable model is different from the standard k-ε model in two important ways, an alternate formulation for turbulent viscosity and a modified transport equation for the dissipation rate. The term realizable means that the model satisfies certain mathematical constraints on the Reynolds stress that neither the standard k-ε model nor the RNG k-ε model satisfies.

#### *3.3.2.3 The k-ω Model*

The most popular alternative to the k- ε model is the k-ω model. In this model the turbulent frequency ω= ε/k is used as the second variable. This model first attracted attention due to the fact that the near wall area of the flow does not require a wall-damping function at low Reynolds numbers. The turbulence kinetic energy k is set to zero at the wall and ω tends to infinity at the wall. This model is good when used in general purpose CFD and external aerodynamics applications, and best for flow over a backward facing step. (Versteeg & Malalasekera, 2007)

The flow equations for k and ω are given in Equation 3.17 and Equation 3.18 respectively.

$$\frac{\partial(\rho k)}{\partial t} + div(\rho k \boldsymbol{U}) = div\left[\left(\mu + \frac{\mu_t}{\sigma_k}\right) grad\ k\right] + \left(2\mu_t S_{ij} \cdot S_{ij} - \frac{2}{3}\rho k \frac{\partial U_i}{\partial x_j}\delta_{ij}\right) - \beta^* \rho\omega \qquad \textbf{[3.17]}$$

$$\frac{\partial(\rho \omega)}{\partial t} + div(\rho \omega \boldsymbol{U}) = div\left[\left(\mu + \frac{\mu_t}{\sigma_\omega}\right) grad\ \omega\right] + \gamma_1\left(2\rho S_{ij} \cdot S_{ij} - \frac{2}{3}\rho\omega \frac{\partial U_i}{\partial x_j}\delta_{ij}\right) - \beta_1 \rho\omega^2 \qquad \textbf{[3.18]}$$

These equations are stated as the rate of change of k or ω plus the transport of k or ω by convection equals the transport of k or ω by turbulent diffusion plus the rate of production of k or ω minus the rate of dissipation of k or ω. The values of the constants for Equation 3.17 and Equation 3.18 are given by $\sigma_k$ = 2.0, $\sigma_\omega$ = 2.0, $\gamma_1$ = 0.533, $\beta_1$ = 0.075, and $\beta^*$ = 0.09. These equations are similar to those given by the k-ε model with the larges t difference being in the terms for production and dissipation of k or ω.

# 4 Chapter Four: Model Construction

## 4.1 Model Construction

Each of the models were constructed using the SpaceClaim software that comes with the ANSYS package. Table 4.1 shows the values that were used for each model. The only difference between the verification model and each of the test models is that the verification model does not model a production tubing string. Instead it models the wellbore region as a solid 7in casing string through the whole interval. This allows for comparison with the inflow performance equations as they are based on the same assumption, as will be shown later.

| | | | |
|---|---|---|---|
| Reservoir Radius | $r_e$ | 5 | ft |
| Wellbore Radius | $r_w$ | 0.583 | ft |
| Casing OD | - | 0.583 | ft |
| Casing ID | - | 0.523 | ft |
| Tubing OD | - | 0.291 | ft |
| Tubing ID | - | 0.249 | ft |
| Upper Reservoir Height | $h_1$ | 2 | ft |
| Lower Reservoir Height | $h_2$ | 2 | ft |

**Table 4.1 Basic Model Properties**

Each subsequent model was based on the same two layer setup with the only changes coming in the diameter of the production tubing and/or the method by which the fluid flows from the annulus to the production tubing string in the upper reservoir i.e. mandrel diameter or sliding sleeve completion option.

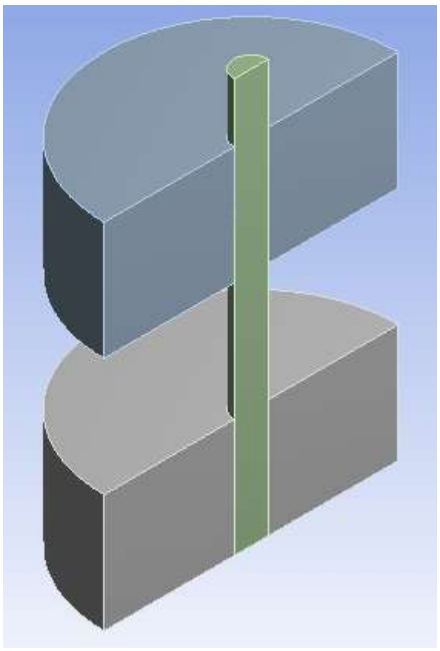

**Figure 4.1 Validation Model Design Split in Half for Detail**

Each test model was based on the verification model with the tubing size changes being from 3.5 inch tubing to 4.5 inch tubing or 2.875 inch tubing. These models were also tested with different orifice sizes for the mandrels with the default for the base case being 0.75in and being sized down from there.

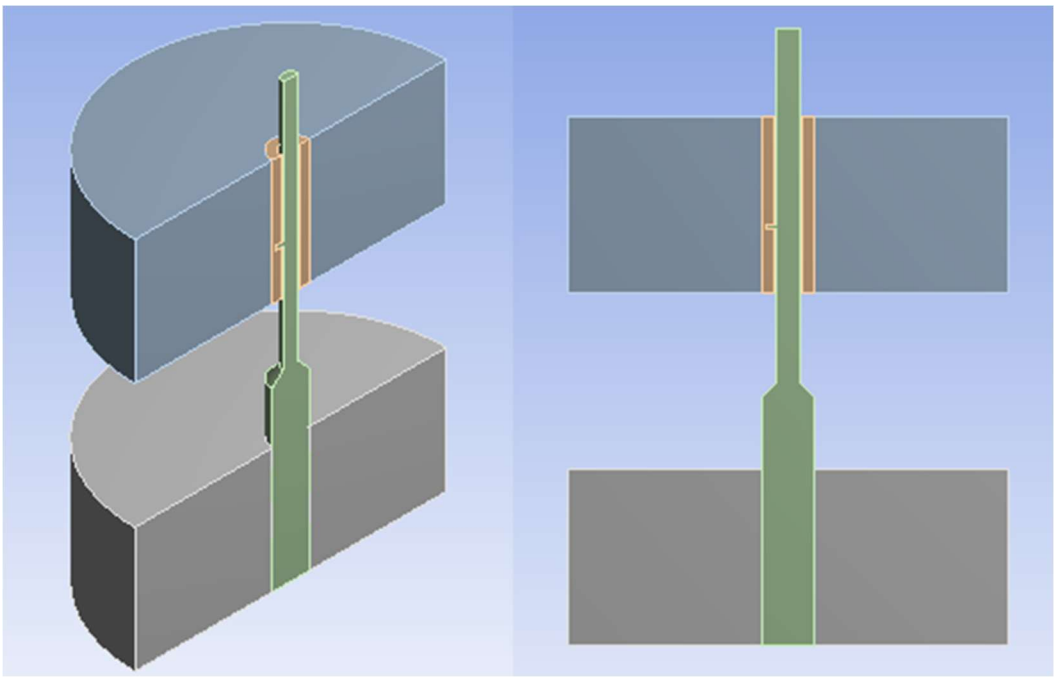

**Figure 4.2 Sample Test Model Split in Half for Detail**

## 4.2 Meshing Overview

The meshing process is where the model is turned from a 3D rendering into a model that the Fluent program can use to determine the flow characteristics of the model. The meshing process takes the 3d rendering and divides it up into smaller nodes to be used for processing. The ANSYS program provides meshing software as part of the package and it was used to generate the mesh for all of the models. This process is done automatically with the only changes being made to the defaults in the program being that the relevance center was set to fine, the span angle center was set to fine, and the quality was set to high. Beyond that the only other steps performed in the meshing program was to label the inlet and outlet faces in the model for use in the Fluent program.

The software generates a mesh based on an inputted 3D model and will show different results based on the size and interactions of each of the components of the model. The academic version of the ANSYS software is limited to 512,000 nodes in the mesh, which is the reason for the small size and symmetry plane of the model. These features will allow for a more detailed meshing around the mandrel and sliding sleeve sections of the models for better accuracy in the calculations.

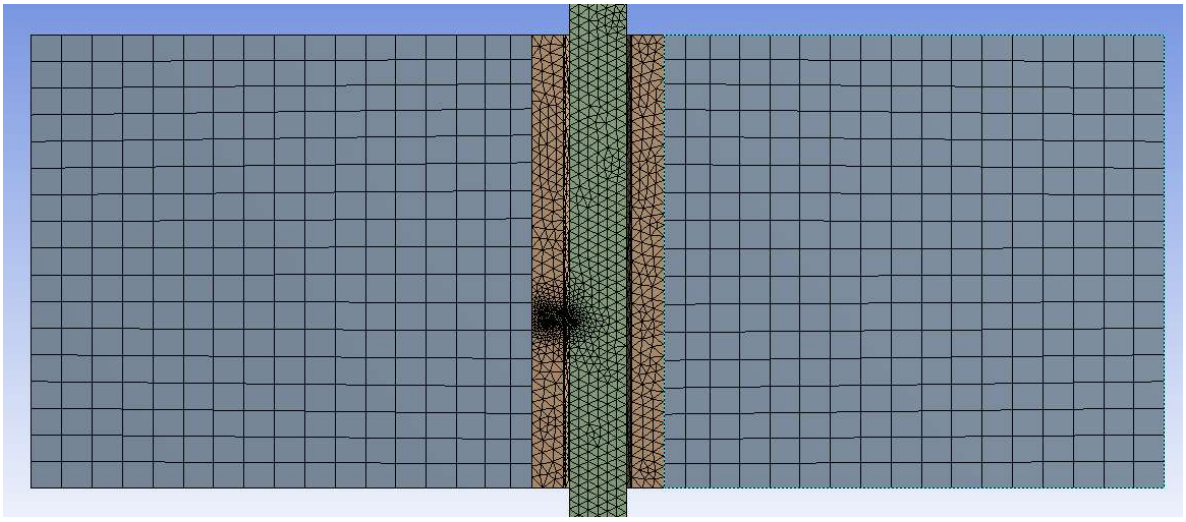

**Figure 4.3 Upper Reservoir Meshing**

The quality of the mesh can be checked with the Fluent program and is referred to as the orthogonality of the mesh. This is accomplished by calculating the normalized dot product of the area vector of a face and a vector from the centroid of the cell to the centroid of that face, and the normalized dot product of the area of a face and a vector from the centroid of the cell the centroid of the adjacent cell that shares that face. These values are calculated for each face in the model and the minimum value that is calculated for each cell is considered the orthogonality of the cell with a value closer to one being best.

The aspect ratio is another indicator of quality and is a measure of the stretching of the cell. It is computed as the ratio of the minimum to maximum value of either the distance between the cell centroid and the face centroids or the distance between the cell centroid and the nodes. Fluent will calculate both the orthogonal quality and the aspect ratio value by asking it to report the quality under setup-general-report quality. Using this command will result in an output showing the minimum orthogonal quality and the maximum aspect ratio of the model (ANSYS, 2013a).

## 4.3 Fluent Setup

The Fluent setup process is fairly straightforward and does not take a long time to complete. Upon starting the Fluent program a window will appear and the double precision check box under options needs to be checked along with the parallel option selected under processing options with the processes being adjusted to 4. The double precision option is best used in models that have long thin pipes and multiple enclosures that are connected by small diameter pipes (ANSYS, 2013a), both of which are present in these models.

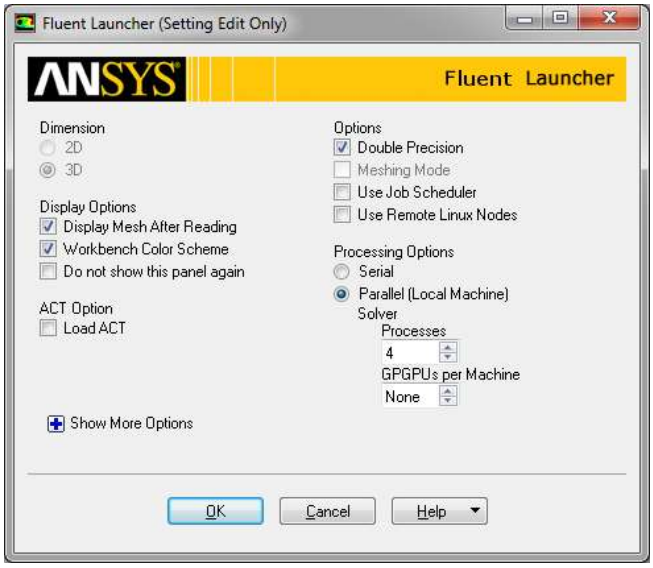


**Figure 4.4 Initial Fluent Setup Options**

The first step is to set the units that will be used in the model. It is important to check each unit, as just selecting the SI or British default may not result in the units being used that are needed. Since oil field units will be used in the models it is important to go through and change the units to the proper setup. Table 4.2 shows which units were changed and what they were changed to.

| Unit | Original Units | Thesis Units |
|---|---|---|
| Acceleration | m/s2 | ft/s2 |
| Area | m2 | ft2 |
| Density | kg/m3 | lbm/ft3 |
| Depth | m | ft |
| Length | m | ft |
| Mass | kg | lbm |
| Mass-Flow Rate | kg/s | lbm/s |
| Pressure | pa | psi |
| Temperature | k | f |
| Velocity | m/s | ft/s |
| Viscosity | kg/m-s | poise |
| Volume | m3 | ft3 |
| Volume-Flow Rate | m3/s | ft3/s |

**Table 4.2 Fluent Units**

After the units have been changed then the next step is to select the turbulence model to be used. The realizable k-ε model with scalable wall functions will be used for each of the models. From here the fluid properties need to be set by either using one of the fluids in the default library or in this case setting a new fluid with a density of 58.253lbm/ft$^3$ and a viscosity of 2.5cp.

The next step in the setup process is to define what fluid is in each zone of the model. This is done by setting all of the zones as the oil fluid created in the previous step. After the fluid is defined for each zone the porous zones need to be set up for both the upper and lower reservoir. The Fluent program uses viscous resistance in units of $1/m^2$ for the permeability and is given by

$$viscous\ resistance\ = \frac{1}{k * 9.9 * 10^{-16}} \quad \textbf{[4.1]}$$

where k is permeability in md. The value of viscous resistance and the porosity are entered into the porous zone section of the cell zone conditions box for the reservoirs. All other settings in the porous zone selection box are left as default.

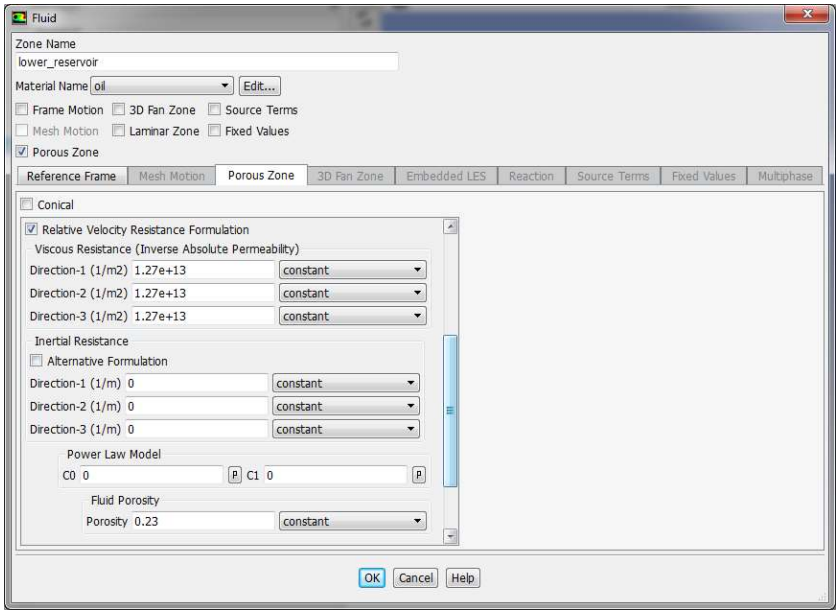


**Figure 4.5 Porous Zone Settings**

Boundary conditions are set next for the inlet and outlet. The upper and lower inlets are set as pressure inlets with both the gauge total pressure and the supersonic/initial gauge pressure being set to 3300 psi. This sets the constant pressure boundary on the reservoir at the desired reservoir pressure. The outlet needs to be set as a pressure outlet with the gauge pressure being set to the flowing bottom hole pressure that is calculated for the model. Again all other setting are left as default for these models.

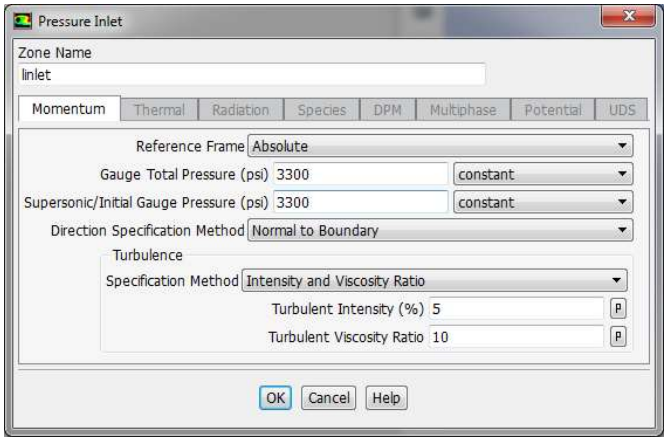


**Figure 4.6 Pressure Inlet Settings**

Under the methods tab, the momentum, turbulent kinetic energy, and turbulent dissipation rate need to be set to second order upwind as is suggested by Fluent. The pressure needs to be set to PRESTO! as it is best suited for steep pressure gradients (ANSYS, 2013a). Initializing the solution is the next step and is done by the standard initialization method by setting all of the values to zero except gauge pressure, set to the boundary pressure of 3300psi and turbulent kinetic energy and dissipation rate, which should be set to 1.

From here the calculations can be run and changes can be made to the model, mesh, and setup of the solver if convergence is not reached. Conveyance is determined when all of the variables being calculated reach a specific threshold but is not a complete indicator the model successfully completed its computations. After convergence is reached, the results must be analyzed and then a determination made that the model has behaved as expected and shows pressures and flow rates in the acceptable range. If convergence is not reached then the convergence criteria can be adjusted in the residuals tab under solving-reports-residuals. Each variable can be adjusted to converge at a higher or lower value, default is set to $10^{-3}$, or is set to be ignored as a convergence criteria.

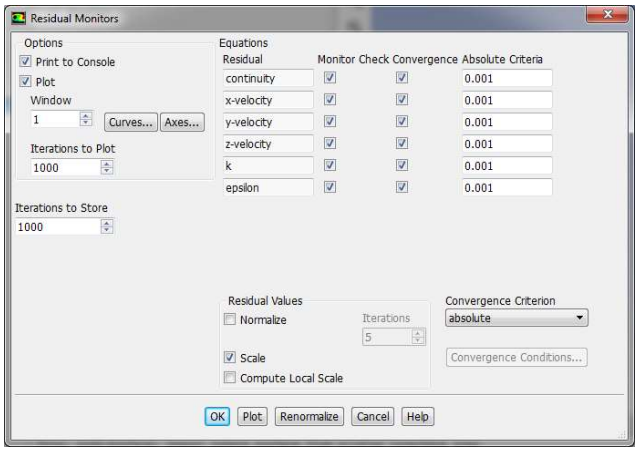


**Figure 4.7 Residuals Monitor**

# 5 Chapter Five: Results and Discussion

## 5.1 Verification Model

Laminar vs turbulent flow regime is simple to calculate but the results play a large role in the overall CFD model. To determine if the flow is laminar or turbulent the Reynolds number needs to be calculated. The Reynolds number is a ratio of the inertial force to the viscous force in a flowing fluid. Equation 5.1 shows how the Reynolds number is calculated.

$$N_{Re} = \frac{Du\rho}{\mu} \quad \textbf{[5.1]}$$

Laminar flow occurs when the fluid flows in parallel layers with no flow perpendicular to the flow direction and no eddy currents, whereas turbulent flow is characterized by changes in pressure and flow velocity. To calculate if the flow is laminar or turbulent in a well we need to know the cross sectional area of the pipe the fluid is flowing in, the density of the fluid, the fluid viscosity, and the flow rate of the fluid. Equation 5.2 shows the combination of this information and Equation 5.1 and conversion to oilfield units.

$$N_{Re} = \frac{1.48q\rho}{D\mu} \quad \textbf{[5.2]}$$

The differentiating line between laminar and turbulent flow is generally considered to be at a Reynolds number of 2100.

Henry Darcy described the flow of fluids in porous media in 1856 by experimenting with water flow through packed sand beds (Darcy, 1856). Darcy was able to determine from his experiments that the pressure drop across the porous sand beds was proportional to the flow rate and inversely proportional to the fluid viscosity. From this Darcy defined permeability and produced

$$q = \frac{kA}{\mu}\frac{dp}{dr} \quad \textbf{[5.3]}$$

Equation 5.3 is given in radial coordinates where q is volumetric flow rate, A is radial area at a distance r and given by $A=2\pi rh$, μ is the dynamic viscosity, and k is the permeability.

Taking Equation 5.3, assuming q is constant, integrating both sides, and converting to oil field units results in Equation 5.4 where P is the pressure at the boundary, $P_{wf}$ is the sand face pressure, r is the radial extent of the well, and $r_w$ is the radius of the wellbore.

$$p - p_{wf} = \frac{q\mu}{2\pi kh} \ln \frac{r}{r_w} \quad [5.4]$$

Using Equation 5.4 the expected flow rate can be calculated for the base model to compare with the results from the CFD model. Table 5.1 gives the input values that will be used for the calculation

| | |
|---|---|
| p (psi) | 3300 |
| μ (cp) | 2.5 |
| k (md) | 80 |
| h (ft) | 2 |
| r (ft) | 2.5 |
| $r_{w\ (ft)}$ | 0.2915 |

**Table 5.1 Base Model Variables**

The model was run using these parameters and using a flowing bottom hole pressure ranging from 0 psi to 3000 psi. The results are shown in

| Lower Reservoir | | | | |
|---|---|---|---|---|
| Pwf [psi] | q From Equation [bbl/d] | Volume Flow Rate [ft/s] | q From Model [bbl/d] | Percentage Difference [%] |
| 0 | 696.02 | 0.0449 | 691.15 | 0.7002 |
| 500 | 590.56 | 0.0381 | 586.42 | 0.7006 |
| 1000 | 485.10 | 0.0313 | 481.70 | 0.7011 |
| 1500 | 379.65 | 0.0245 | 376.98 | 0.7021 |
| 2000 | 274.19 | 0.0177 | 272.26 | 0.7032 |
| 2500 | 168.73 | 0.0109 | 167.54 | 0.7052 |
| 3000 | 63.27 | 0.0041 | 62.83 | 0.7102 |

Table 5.2 and

| Upper Reservoir | | | | |
|---|---|---|---|---|
| Pwf [psi] | q From Equation [bbl/d] | Volume Flow Rate [ft/s] | q From Model [bbl/d] | Percentage Difference [%] |
| 0 | 783.02 | 0.0507 | 779.75 | 0.4180 |
| 500 | 664.38 | 0.0430 | 661.61 | 0.4170 |
| 1000 | 545.74 | 0.0353 | 543.47 | 0.4158 |
| 1500 | 427.10 | 0.0276 | 425.33 | 0.4144 |
| 2000 | 308.46 | 0.0200 | 307.19 | 0.4118 |
| 2500 | 189.82 | 0.0123 | 189.05 | 0.4089 |
| 3000 | 71.18 | 0.0046 | 70.89 | 0.4130 |

Table 5.3 along with the expected results from Equation 5.4 for both the lower and upper reservoirs respectively.

| Lower Reservoir | | | | |
|---|---|---|---|---|
| Pwf [psi] | q From Equation [bbl/d] | Volume Flow Rate [ft/s] | q From Model [bbl/d] | Percentage Difference [%] |
| 0 | 696.02 | 0.0449 | 691.15 | 0.7002 |
| 500 | 590.56 | 0.0381 | 586.42 | 0.7006 |
| 1000 | 485.10 | 0.0313 | 481.70 | 0.7011 |
| 1500 | 379.65 | 0.0245 | 376.98 | 0.7021 |
| 2000 | 274.19 | 0.0177 | 272.26 | 0.7032 |
| 2500 | 168.73 | 0.0109 | 167.54 | 0.7052 |
| 3000 | 63.27 | 0.0041 | 62.83 | 0.7102 |

**Table 5.2 Lower Reservoir Flow Rates**

| Upper Reservoir | | | | |
|---|---|---|---|---|
| Pwf [psi] | q From Equation [bbl/d] | Volume Flow Rate [ft/s] | q From Model [bbl/d] | Percentage Difference [%] |
| 0 | 783.02 | 0.0507 | 779.75 | 0.4180 |
| 500 | 664.38 | 0.0430 | 661.61 | 0.4170 |
| 1000 | 545.74 | 0.0353 | 543.47 | 0.4158 |
| 1500 | 427.10 | 0.0276 | 425.33 | 0.4144 |
| 2000 | 308.46 | 0.0200 | 307.19 | 0.4118 |
| 2500 | 189.82 | 0.0123 | 189.05 | 0.4089 |
| 3000 | 71.18 | 0.0046 | 70.89 | 0.4130 |

**Table 5.3 Upper Reservoir Flow Rates**

These results show that the CFD model produced the same flow rates as expected within 0.5% for the upper reservoir and 0.8% for the lower reservoir for all flow rates tested. These values are presented in reservoir barrels instead of using formation volume factor to convert them to stock tank barrels.

Equation 5.4 gives the steady state, meaning the pressure and fluid saturation at any point in the system react instantaneously to the changes (Craft & Hawkins, 1991); flow rate from the reservoir assuming no skin is present. Skin is the area of steady-state pressure difference in the near wellbore region as described by Vaneverding and Hurst (VanEverdingen & Hurst, 1949). This model is not concerned with measuring different flow characteristics due to skin created by perforations, formation damage, or any of the other numerous reasons skin can occur in wells. For this reason an openhole completion type was mimicked for each of the models, thus leaving the entire reservoir face open to the

wellbore for production. While this is not the true case for what is happening in most of the wellbores, it is a fair representation for comparison of each model to the verification model.

The inflow performance relationship (IPR) curve is only half of what is needed to determine deliverability from a well. Vertical lift performance (VLP) curves also need to be generated to determine what the flowing bottom hole pressure will be based on wellhead pressure. To determine the VLP the pressure drop needs to be determined over the length of the well. The mechanical energy balance equation needs to be solved to determine the pressure drop over a distance L for a single phase flow as shown in Equation 5.5.

$$\frac{dp}{\rho} + \frac{udu}{g_c} + \frac{g}{g_c}dz + \frac{2f_f u^2 dL}{g_c D} + dW_s = 0 \quad \textbf{[5.5]}$$

With an incompressible fluid and no pumps, compressors, or turbines in the line the equations becomes.

$$\Delta p = \frac{g}{g_c}\rho\Delta z + \frac{\rho}{2g_c}\Delta u^2 + \frac{2f_f \rho u^2 L}{g_c D} \quad \textbf{[5.6]}$$

The terms on the right hand side of Equation 5.6 are potential energy, kinetic energy, and frictional pressure drop. Knowing that the only pipe size change in the well is where the fluid enters the tubing from the casing, and that the pressure needed for the model is above all of the inlets for the system, the kinetic energy term can be ignored leaving only the potential energy term and the frictional pressure drop given by

$$\Delta p_{pe} = \frac{g}{g_c}\rho\Delta z \quad \textbf{[5.7]}$$

$$\Delta p_f = \frac{2f_f u^2 L}{g_c D} \quad \textbf{[5.8]}$$

Equation 5.7 can be simplified by computing the pressure drop for water over one foot and then multiplying it by the specific gravity of the desired fluid $\gamma_w$. To convert $\frac{g}{g_c}$ to the gradient for water divide the density of water by 144in$^2$ to convert 62.4 lbm/ft$^3$ to 0.433 psi/ft.

$$\Delta p_{pe} = 0.433\gamma_w\Delta z \quad \textbf{[5.9]}$$

$\Delta z$ in this case, since the well is vertical, is simply the depth of the well, 3500'. The potential energy drop for the verification model, using 0.938 for $\gamma_w$, is calculated to be approximately 1422 psi.

The frictional pressure drop is more complicated to calculate and requires the solving of the Fanning equation

$$\Delta p_F = \frac{2 f_f \rho u^2 L}{g_c D} \quad \textbf{[5.10]}$$

Given that $f_f$ is the fanning friction factor which is a simple function of the Reynolds number for laminar flow.

$$f_f = \frac{16}{N_{Re}} \quad \textbf{[5.11]}$$

For turbulent flow the calculation of the friction factor uses the Chen equation (Chen, 1979)

$$\frac{1}{\sqrt{f_f}} = -4 \log\left\{\frac{\varepsilon}{3.7065} - \frac{5.0452}{N_{Re}} \log\left[\frac{\epsilon^{1.1098}}{2.8257} + \left(\frac{7.149}{N_{Re}}\right)^{0.8981}\right]\right\} \quad \textbf{[5.12]}$$

Where ε is the relative roughness and $N_{Re}$ is the Reynolds number. Using Equation 5.11 the friction factor $f_f$ of the system is determined and plugged into Equation 5.12, assuming a value of 0.001 for ε, 3000 for $N_{Re}$, and 500 bbl/day for q, to arrive at 0.435 psi for the friction pressure drop. It can be seen that this value is much smaller than the potential energy pressure drop and is often times ignored in simple calculations due to the complexity in calculating the value.

The calculation of the VLP curve is done for each flow rate that is available for the IPR curve and plotted on the same chart to arrive at the optimal flowing bottom hole pressure (FBHP), $p_{wf}$. The point where the IPR and VLP curves cross is considered the optimal FBHP for the system. If the flowing wellhead pressure (FWHP) is changed for the system then the VLP curve will move higher on the chart and the optimal flow rate for the well will decrease. For the verification model a FWHP of 0 psi was selected. This value, while not realistic due to backpressure from the surface gathering systems, was selected to simplify the calculations. Figure 5.1 shows the overlay of the IPR curve and the VLP curve for the verification model.

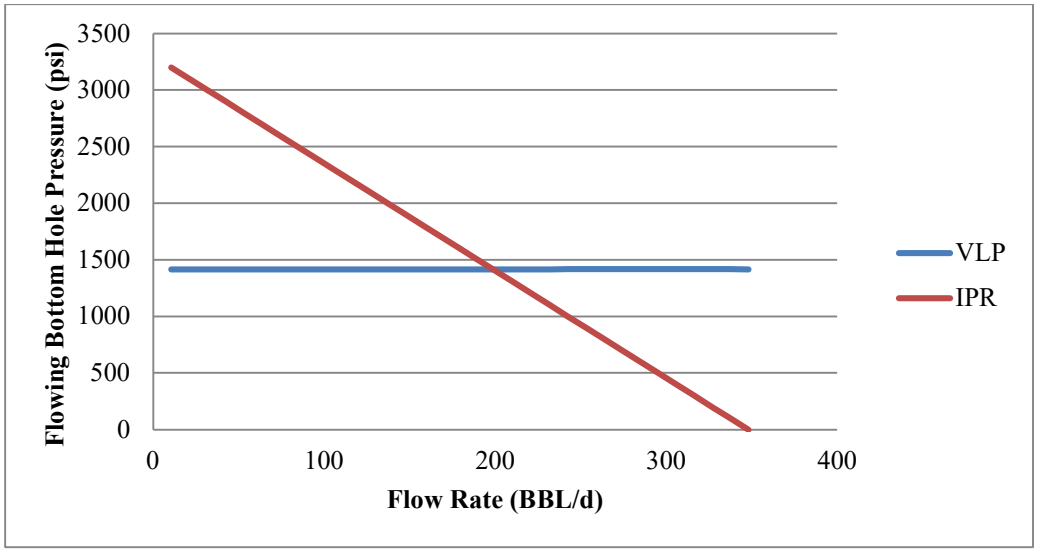


**Figure 5.1 IPR-VLP Chart for validation model**

This process can be iterative but with a good initial guess for flow rate and Reynolds number the number of iterations should be small if needed at all. Small changes in the Reynolds number have small effects one the friction factor, and since this number is a fraction of the total pressure drop it has hardly any effect on calculating the bottom hole pressure as long as the initial guess is close to the actual value. Figure 5.2 shows that for the base case the flow is turbulent when it is above 182 bbl/day and laminar when it is below that value. Since the flowing bottom hole pressure is 1422 psi and the flow rate is roughly 400 bbl/d it is safe to assume that the turbulent regime will dominate the flow in the wellbore area.

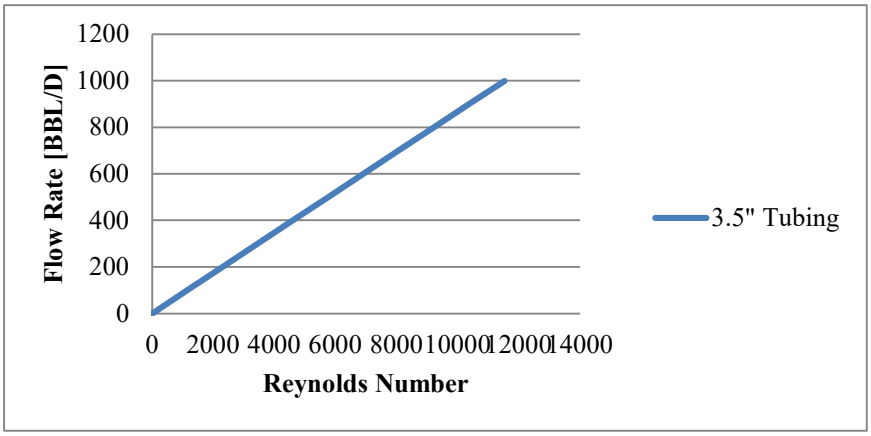


**Figure 5.2 Reynolds number for verification model**

If the tubing size is changed then the Reynolds number will change accordingly as can be seen in Figure 5.3. For all of the cases that will be looked at, the flow is shown to be turbulent in the wellbore, so the realizable k-ε model was selected.

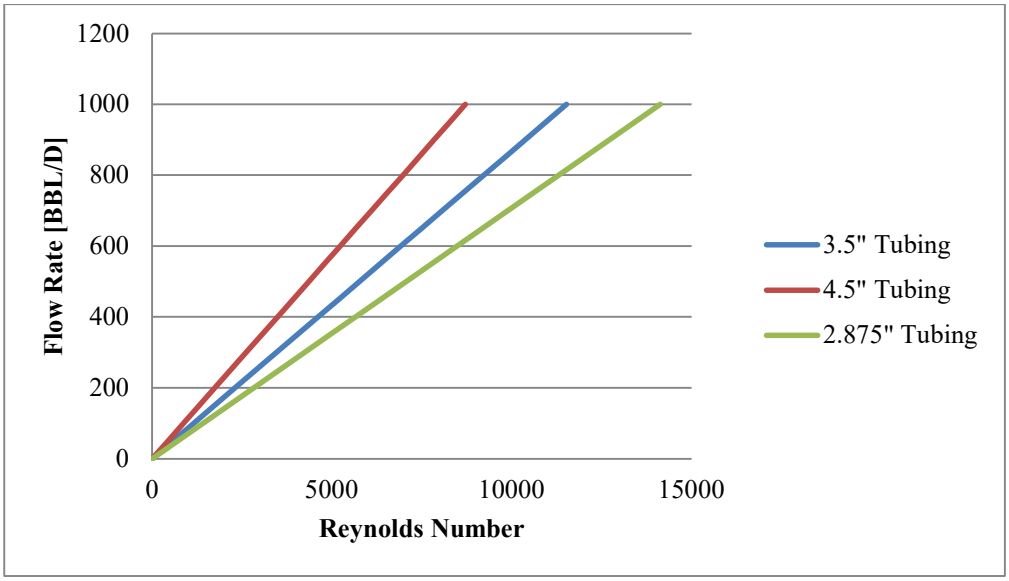


**Figure 5.3 Reynolds number for all cases**

## 5.2 Mandrel Model

### 5.2.1 Base Model

A base model was created for each of the three tubing strings to be examined. These base models differed from the verification model in the fact that they did not show a 7 inch casing string through both reservoirs. At the mid-point between the two reservoirs the 7 inch casing string was tapered into one of three common sized tubing stings, 4.5 inch, 3.5 inch, or 2.875 inch. The space between the reservoir and the tubing string was composed of an annulus area that was connected openhole style to the upper reservoir in the same way the verification model was. The connection from the annulus to the tubing was made up of a 0.75 inch port to mimic an orifice valve. Figure 5.4 shows a close up view of this section of the model.

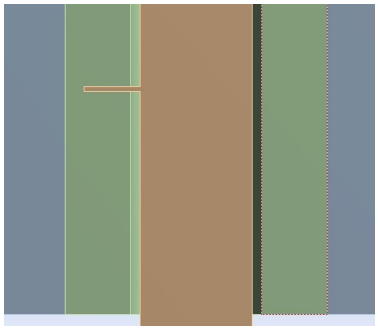

**Figure 5.4 Close up of Valve Area**

This base case was run as a comparison to the validation model to determine if the simple act of putting the valve in between the reservoir and the tubing would cause a reduced production from the

upper reservoir. Table 5.4 and Table 5.5 show the results of each of the three models compared to the validation model from the upper and lower reservoir respectively.

| Upper Reservoir | | | | |
|---|---|---|---|---|
| Pwf [psi] | Validation Model Percentage Difference [%] | 2.875" Model Percentage Difference [%] | 3.5" Model Percentage Difference [%] | 4.5" Model Percentage Difference [%] |
| 0 | 0.4180 | 0.5541 | 0.6074 | 0.7082 |
| 500 | 0.4170 | 0.5439 | 0.5893 | 0.7069 |
| 1000 | 0.4158 | 0.5206 | 0.5582 | 0.6768 |
| 1500 | 0.4144 | 0.5061 | 0.5516 | 0.6720 |
| 2000 | 0.4118 | 0.4887 | 0.5346 | 0.6759 |
| 2500 | 0.4089 | 0.4711 | 0.5181 | 0.6521 |
| 3000 | 0.4130 | 0.4554 | 0.5022 | 0.6578 |

**Table 5.4 Upper Reservoir Base to Validation Comparison**

| Lower Reservoir | | | | |
|---|---|---|---|---|
| Pwf [psi] | Validation Model Percentage Difference [%] | 2.875" Model Percentage Difference [%] | 3.5" Model Percentage Difference [%] | 4.5" Model Percentage Difference [%] |
| 0 | 0.7002 | 0.6600 | 0.7224 | 0.6072 |
| 500 | 0.7006 | 0.6672 | 0.6578 | 0.7493 |
| 1000 | 0.7011 | 0.6497 | 0.6280 | 0.5824 |
| 1500 | 0.7021 | 0.6540 | 0.6349 | 0.6896 |
| 2000 | 0.7032 | 0.6433 | 0.6446 | 0.6495 |
| 2500 | 0.7052 | 0.6438 | 0.6406 | 0.6151 |
| 3000 | 0.7102 | 0.6460 | 0.6498 | 0.5722 |

**Table 5.5 Lower Reservoir Base to Validation Comparison**

This data shows that there is no significant reduction in the production from the upper or lower reservoir from the addition of the tubing string or the valve. This will allow for each of the models to be tested with valve sizes of 0.5, 0.375, 0.25, and 0.125 inches to determine if there is a reduction in the production from the upper reservoir.

### 5.2.2 Well 1: 2.875 inch Model

#### *5.2.2.1 Flow Rate Characteristics*

The lower reservoir is only constrained by the tubing or fluid flow from the upper reservoir. Since the lower reservoir is able to flow full open in the validation model and in the base case for the 2.875 inch tubing size it will not be affected by the changing of the valve size for the upper reservoir. Table 5.6 gives the percentage difference for each case compared to the base case and it can be seen that the results are as expected. The only difference in each case is due to variations in the computation for that model and all are within 0.3% of each other.

| Lower Reservoir | | | | | |
|---|---|---|---|---|---|
| Pwf [psi] | Base Model Percentage Difference [%] | Case 1 Percentage Difference [%] | Case 2 Percentage Difference [%] | Case 3 Percentage Difference [%] | Case 4 Percentage Difference [%] |
| 0 | 0.6600 | 0.6051 | 0.6039 | 0.5048 | 0.6601 |
| 500 | 0.6672 | 0.9596 | 0.2429 | 0.6328 | 0.6373 |
| 1000 | 0.6497 | 0.5152 | 0.3480 | 0.6791 | 0.6248 |
| 1500 | 0.6540 | 0.6291 | 0.6264 | 0.6210 | 0.6482 |
| 2000 | 0.6433 | 0.6264 | 0.5141 | 0.5429 | 0.6607 |
| 2500 | 0.6438 | 0.6724 | 0.4762 | 0.8323 | 0.6412 |
| 3000 | 0.6460 | 0.6554 | 0.6486 | 0.6426 | 0.6978 |

**Table 5.6 2.875" Model Lower Reservoir Flow Rate Comparison**

The upper reservoir is where the reduction in production is expected to occur. Figure 5.5 shows a plot of pressure vs flow rates for each of the cases.

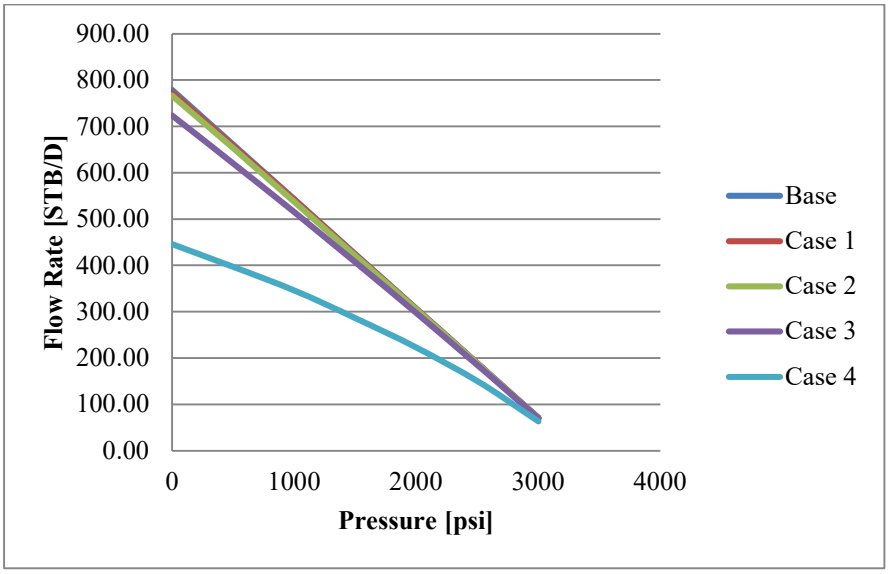


**Figure 5.5 2.875 inch Upper Reservoir Flow Rates**

The flow rates show little movement off of the base case for the first two cases, 0.5 and 0.375 inch valves. It takes the 0.25 inch valve to start to make a difference in the flow rate. The flow rates and percentage difference are shown in Table 5.7 and Table 5.8 for the 0.5 and 0.375 inch valves respectively.

| Upper Reservoir | | | | |
|---|---|---|---|---|
| Pwf [psi] | q From Equation [bbl/d] | Volume Flow Rate [ft/s] | q From Model [bbl/d] | Percentage Difference [%] |
| 0 | 783.02 | 0.0503 | 774.22 | 1.1247 |
| 500 | 664.38 | 0.0428 | 658.30 | 0.9157 |
| 1000 | 545.74 | 0.0352 | 542.03 | 0.6798 |
| 1500 | 427.10 | 0.0275 | 423.90 | 0.7507 |
| 2000 | 308.46 | 0.0199 | 306.43 | 0.6584 |
| 2500 | 189.82 | 0.0123 | 188.71 | 0.5861 |
| 3000 | 71.18 | 0.0046 | 70.84 | 0.4874 |

**Table 5.7 2.875" Case 1 Flow Rates**

| Upper Reservoir | | | | |
|---|---|---|---|---|
| Pwf [psi] | q From Equation [bbl/d] | Volume Flow Rate [ft/s] | q From Model [bbl/d] | Percentage Difference [%] |
| 0 | 783.02 | 0.0498 | 766.83 | 2.0675 |
| 500 | 664.38 | 0.0424 | 653.08 | 1.7005 |
| 1000 | 545.74 | 0.0349 | 537.22 | 1.5621 |
| 1500 | 427.10 | 0.0274 | 421.52 | 1.3065 |
| 2000 | 308.46 | 0.0198 | 305.21 | 1.0546 |
| 2500 | 189.82 | 0.0122 | 188.29 | 0.8065 |
| 3000 | 71.18 | 0.0046 | 70.76 | 0.5885 |

**Table 5.8 2.875" Case 2 Flow Rates**

As will be seen in all of the cases the high flow rates will produce a larger percentage of difference from the base case. In case 1, the 0.5 inch valve, there is only a 1.1% difference I the flow rates from the base case at the lowest drawdown pressure of zero psi. The second drawdown pressure of 500 psi shows a 0.9% difference over the base case and all of the pressures from 1000 psi to 3000 psi show the same general percentage difference as the base case does from the calculated IPR data. Case 2, the 0.375 inch valve, shows slightly more difference in the flow rate at lower pressures with the drawdown pressure of zero being the largest difference at 2.0%. At the pressure closest to the predicted pressure the well will flow at, 1500 psi, we see the difference of 1.3% over the base model.

| Upper Reservoir | | | | |
|---|---|---|---|---|
| Pwf [psi] | q From Equation [bbl/d] | Volume Flow Rate [ft/s] | q From Model [bbl/d] | Percentage Difference [%] |
| 0 | 783.02 | 0.0470 | 723.73 | 7.5721 |
| 500 | 664.38 | 0.0403 | 620.35 | 6.6270 |
| 1000 | 545.74 | 0.0335 | 514.88 | 5.6549 |
| 1500 | 427.10 | 0.0265 | 407.17 | 4.6659 |
| 2000 | 308.46 | 0.0193 | 297.61 | 3.5194 |
| 2500 | 189.82 | 0.0120 | 185.34 | 2.3627 |
| 3000 | 71.18 | 0.0046 | 70.35 | 1.1678 |

**Table 5.9 2.875" Case 3 Flow Rates**

Table 5.9 shows the data for case 3, the 0.25 inch valve, and it can be seen that this is the first case to start to show larger difference for the flow rates over the validation model. At a drawdown pressure of zero psi we see a 7.6% difference and a at the expected flowing bottom hole pressure of 1500 psi we see a 4.7% difference. Case 4, the 0.125 inch valve, shows the largest difference over the expected calculated IPR values and is shown in Table 5.10. This case shows a maximum percentage difference of 43% at a drawdown pressure of zero and shows 32.9% difference at the expected bottom hole pressure.

| Upper Reservoir | | | | |
|---|---|---|---|---|
| Pwf [psi] | q From Equation [bbl/d] | Volume Flow Rate [ft/s] | q From Model [bbl/d] | Percentage Difference [%] |
| 0 | 783.02 | 0.0290 | 446.01 | 43.0398 |
| 500 | 664.38 | 0.0258 | 397.17 | 40.2193 |
| 1000 | 545.74 | 0.0225 | 346.17 | 36.5694 |
| 1500 | 427.10 | 0.0186 | 286.50 | 32.9207 |
| 2000 | 308.46 | 0.0145 | 222.88 | 27.7465 |
| 2500 | 189.82 | 0.0098 | 150.48 | 20.7254 |
| 3000 | 71.18 | 0.0041 | 63.85 | 10.3069 |

**Table 5.10 2.875" Case 4 Flow Rates**

#### *5.2.2.2 Pressure Characteristics*

Figure 5.6 shows the pressure drawdown for the base case and Figure 5.7 shows the pressure drawdown for each case with the flowing bottom hole pressure of 1500 psi. Case 1 and case 2 do not show much difference from each other in the pressures in the reservoir. Case 3 starts to show a higher pressure in the reservoir region closes to the well bore with the annular region still showing close to 1500 psi. Case 4 shows the largest increase in pressure in the annular and near reservoir region due to the valve

size and flow reduction with the annular region showing a significantly higher pressure than shown in the other three cases.

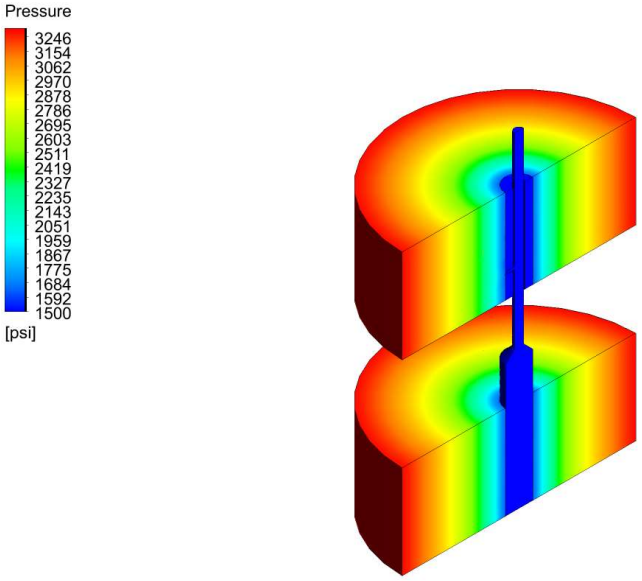


**Figure 5.6 2.875 inch Model Pressure Drawdown for Base Case**

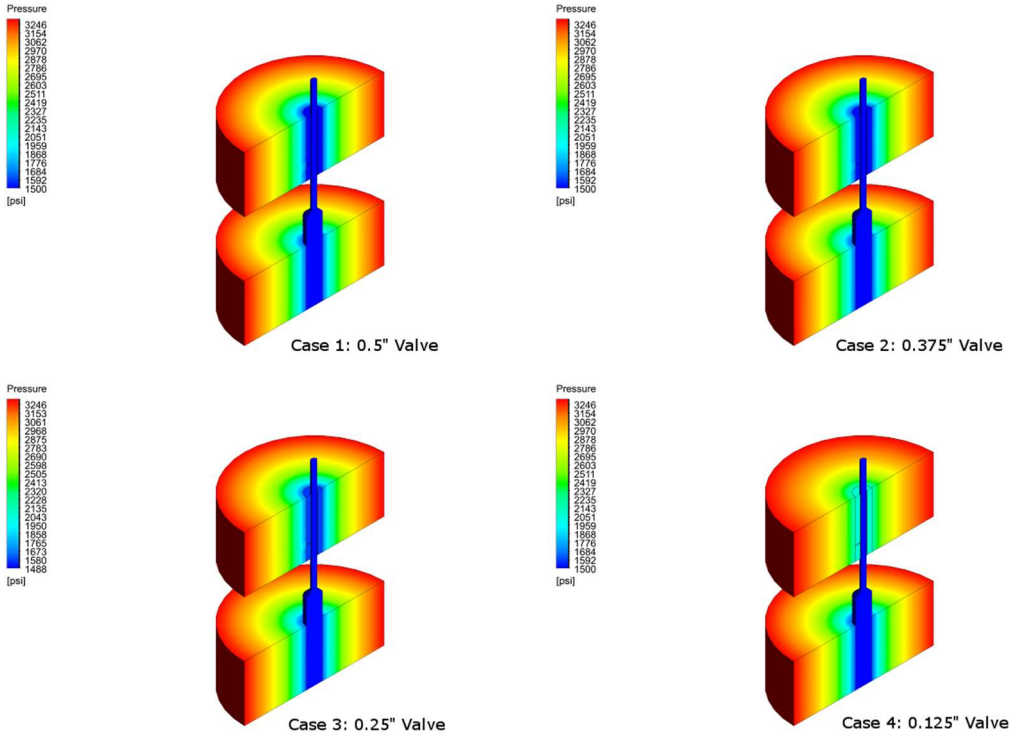


**Figure 5.7 Pressure Drawdown for Each Case**

Looking at the pressures in the wellbore and the reservoir shows exact values for the pressure at the points 0, 0.5, 1.0, 1.5, 2.0, 2.5 feet from the center of the well bore. Table 5.11 shows these values.

| Upper Reservoir | | | | | |
|---|---|---|---|---|---|
| Distance From Center of Wellbore [ft] | Base Model Pressure [psi] | Case 1 Pressure [psi] | Case 2 Pressure [psi] | Case 3 Pressure [psi] | Case 4 Pressure [psi] |
| 0.0 | 1500 | 1500 | 1500 | 1500 | 1500 |
| 0.5 | 1922 | 1947 | 1948 | 1989 | 2344 |
| 1.0 | 2501 | 2503 | 2508 | 2533 | 2758 |
| 1.5 | 2869 | 2870 | 2873 | 2886 | 3007 |
| 2.0 | 3124 | 3125 | 3126 | 3131 | 3181 |
| 2.5 | 3277 | 3277 | 3277 | 3278 | 3284 |

**Table 5.11 Pressure at Distance for Each Case**

The pressures start to climb closer to the wellbore before affecting the region closer to the boundary of the reservoir and it is not until case 4 that the pressure at the boundary is affected. Each step shows a slight increase in the pressures for each distance from the wellbore until case 4 where a larger jump is shown in much the same way as the production data shows a much lower production for case 4 than any other case.

#### *5.2.2.3 Velocity Characteristics*

Looking at the velocity profile of the base case, Figure 5.8, shows that the velocity going through the valve is higher than in any other area of the model.

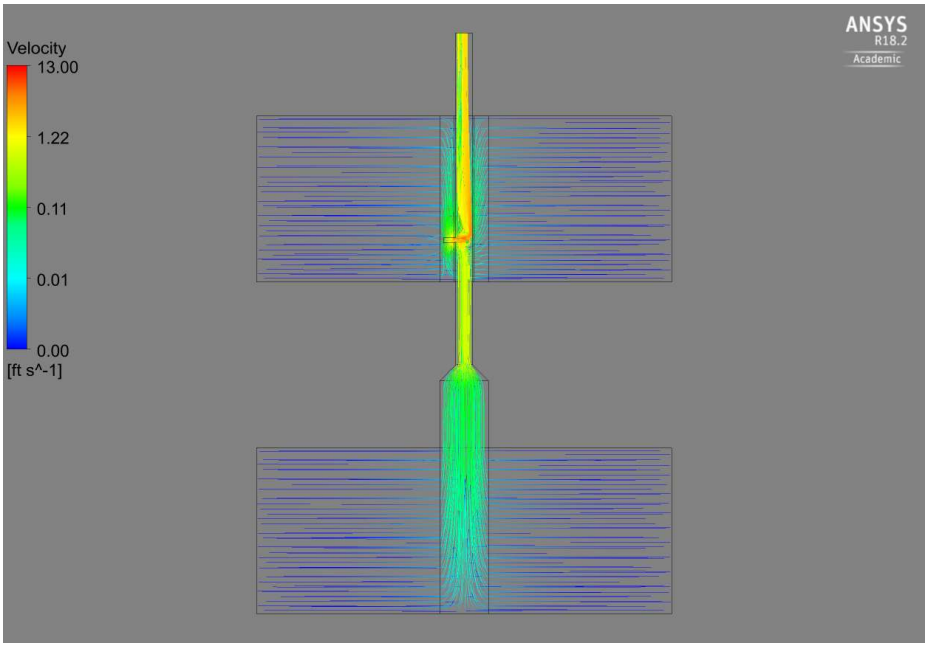


**Figure 5.8 Velocity Streamlines for Base Case**

The streamlines show the path that some of the particles take through the system. The velocity is seen as higher upon entering the tubing than in the casing and higher still once all of the fluid is comingled above the valve. Figure 5.9 shows the velocity profile for each of the cases.

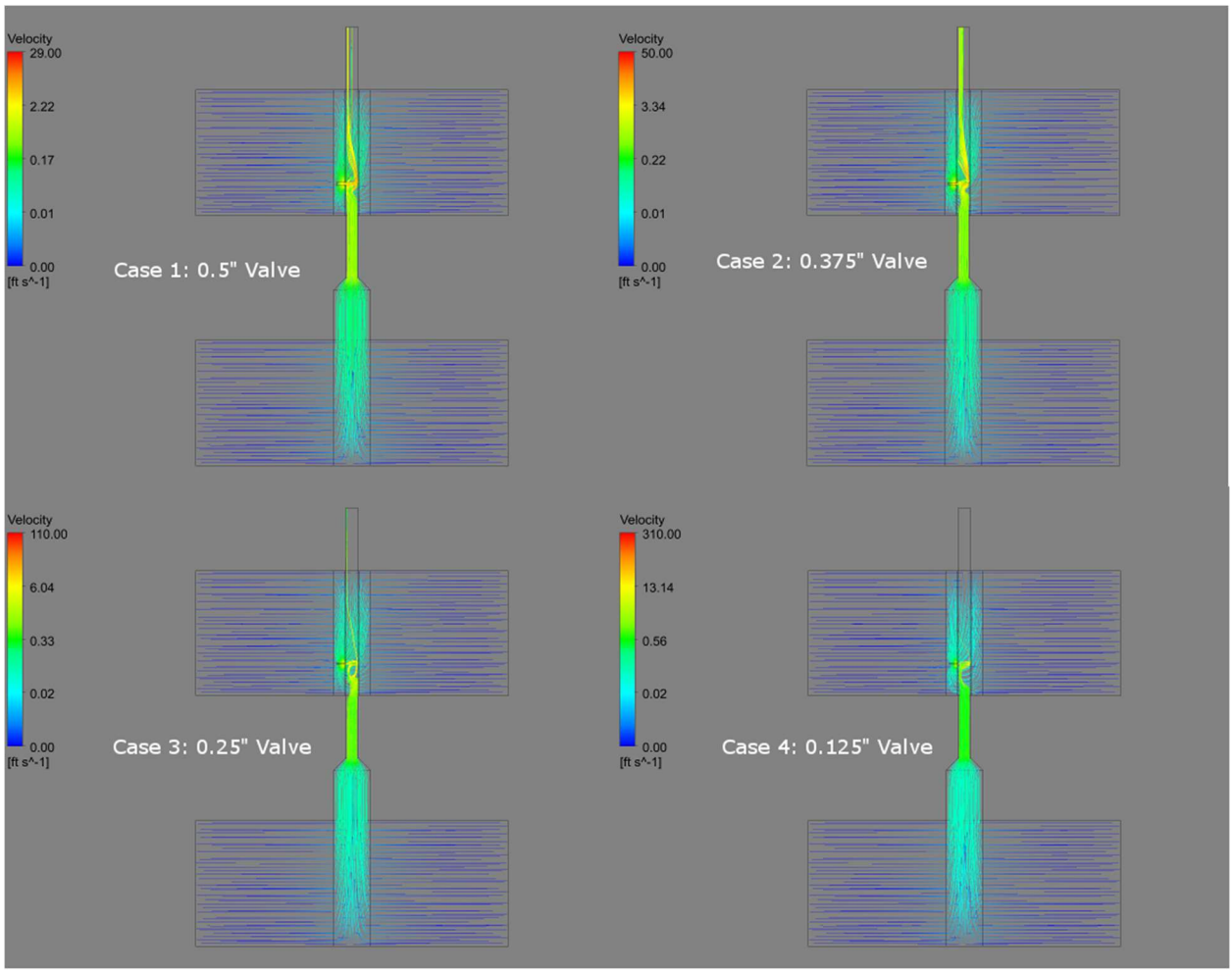


**Figure 5.9 Velocity Profile for Each Case**

With each case the velocity though the valve increases due to the restricted size of the valve. The high velocity seen in case 4 can cause jetting to occur in the valve and in the tubing opposite the valve. This jetting can have adverse effects on the well and could, over time, cause undue wear on the tubing and possible failure of the tubing or valve. If enough of the valve is eroded then the pocket on the mandrel will start to erode with it which would result in losing the ability to isolate the zone. This case would require more monitoring for these effects and result in a higher operational cost on the well. The overall likelihood of running a valve in this situation would have to be evaluated on a well by well basis to determine the fiscal ability to withstand it.

### 5.2.3 Well 2: 3.5 inch Model

#### *5.2.3.1 Flow Rate Characteristics*

Table 5.12 shows the flow rates for each of the four cases compared to the base case. The lower reservoir is again not encumbered by the tubing at any of these flow rates allowing it to flow freely at its maximum rate, with the only difference in each rate being from computational differences in the software similar to the 2.875 inch model. Each of these rates shows a less than 0.3% difference from base model.

| Lower Reservoir | | | | | |
|---|---|---|---|---|---|
| Pwf [psi] | Base Model Percentage Difference [%] | Case 1 Percentage Difference [%] | Case 2 Percentage Difference [%] | Case 3 Percentage Difference [%] | Case 4 Percentage Difference [%] |
| 0 | 0.7224 | 0.6583 | 0.6592 | 0.4676 | 0.6142 |
| 500 | 0.6578 | 0.5688 | 0.8386 | 0.8545 | 0.7352 |
| 1000 | 0.6280 | 0.6116 | 0.7772 | 0.5863 | 0.7984 |
| 1500 | 0.6349 | 0.6161 | 0.5831 | 0.8179 | 0.5870 |
| 2000 | 0.6446 | 0.6426 | 0.6302 | 0.5647 | 0.6393 |
| 2500 | 0.6406 | 0.6721 | 0.9331 | 0.5579 | 0.5982 |
| 3000 | 0.6498 | 0.6443 | 0.7375 | 0.5816 | 0.6721 |

**Table 5.12 3.5" Model Lower Reservoir Flow Rate Comparison**

Figure 5.10 shows the flow rates for the different drawdown pressures of the upper reservoir for each case. This shows a similar trend to the 2.875 inch case in that case 1 and case 2 are within 2% of the base case production with case 1 being almost the same as the base case and case 2 having a little bit lower production. Case 3 again shows a larger decline from the base case with case 4 showing the largest drop off in production compared to the base case.

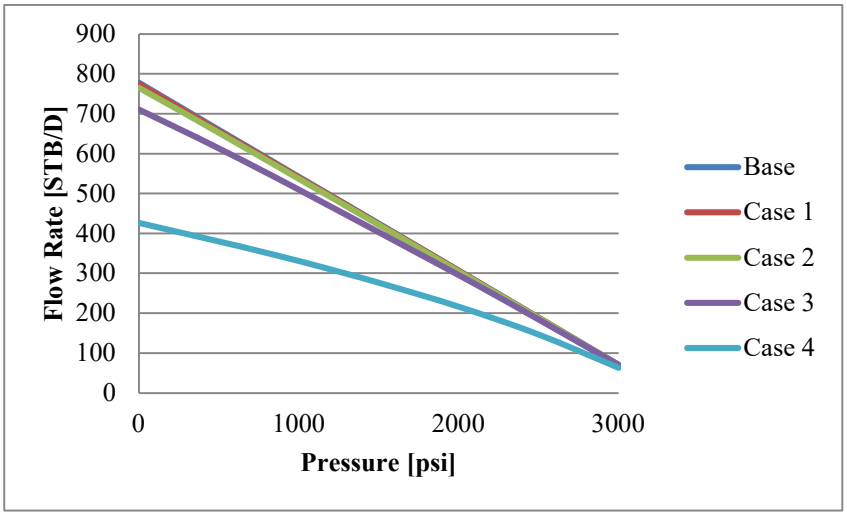


**Figure 5.10 3.5" Model Upper Reservoir Flow Rates**

Table 5.13 and Table 5.14 show the actual calculated flow rates for case 1 and case 2 respectively. Both of these cases show the 2% or less maximum change in production and at the estimated flowing bottom hole pressure of around 1500 psi case 1 shows no appreciable change from the base case and case 2 shows only a 1% drop from the base case. This 1% is likely imperceptible in the ebb and flow of daily production from the well.

| Upper Reservoir | | | | |
|---|---|---|---|---|
| Pwf [psi] | q From Equation [bbl/d] | Volume Flow Rate [ft/s] | q From Model [bbl/d] | Percentage Difference [%] |
| 0 | 783.02 | 0.0504 | 775.08 | 1.0149 |
| 500 | 664.38 | 0.0427 | 657.03 | 1.1073 |
| 1000 | 545.74 | 0.0352 | 541.01 | 0.8681 |
| 1500 | 427.10 | 0.0275 | 423.77 | 0.7795 |
| 2000 | 308.46 | 0.0199 | 306.29 | 0.7044 |
| 2500 | 189.82 | 0.0123 | 188.63 | 0.6303 |
| 3000 | 71.18 | 0.0046 | 70.80 | 0.5422 |

**Table 5.13 3.5" Case 1 Flow Rates**

| Upper Reservoir | | | | |
|---|---|---|---|---|
| Pwf [psi] | q From Equation [bbl/d] | Volume Flow Rate [ft/s] | q From Model [bbl/d] | Percentage Difference [%] |
| 0 | 783.02 | 0.0498 | 765.66 | 2.2176 |
| 500 | 664.38 | 0.0424 | 652.94 | 1.7222 |
| 1000 | 545.74 | 0.0349 | 537.47 | 1.5160 |
| 1500 | 427.10 | 0.0274 | 421.58 | 1.2930 |
| 2000 | 308.46 | 0.0198 | 305.17 | 1.0682 |
| 2500 | 189.82 | 0.0122 | 188.20 | 0.8553 |
| 3000 | 71.18 | 0.0046 | 70.73 | 0.6400 |

**Table 5.14 3.5" Case 2 Flow Rates**

The third case shows a larger drop in production at absolute open flow of a little over 9%, as can be seen in Table 5.15, from the base case. This is on track with case 3 from the 2.875 inch model and shows a drop of 5.5% drop from the base case at the expected 1500 psi. Case 4 is shown in Table 5.16 and shows a much larger prop in production for all of the flow rates than any other cases tested. It shows a maximum drop of 45.5% for the flowing bottom hole pressure of zero and a drop of 35.2% for the 1500 psi flowing bottom hole pressure.

| Upper Reservoir | | | | |
|---|---|---|---|---|
| Pwf [psi] | q From Equation [bbl/d] | Volume Flow Rate [ft/s] | q From Model [bbl/d] | Percentage Difference [%] |
| 0 | 783.02 | 0.0462 | 710.88 | 9.2138 |
| 500 | 664.38 | 0.0399 | 613.66 | 7.6348 |
| 1000 | 545.74 | 0.0331 | 510.08 | 6.5339 |
| 1500 | 427.10 | 0.0262 | 403.42 | 5.5449 |
| 2000 | 308.46 | 0.0192 | 295.96 | 4.0529 |
| 2500 | 189.82 | 0.0120 | 184.64 | 2.7320 |
| 3000 | 71.18 | 0.0046 | 70.22 | 1.3583 |

**Table 5.15 3.5" Case 3 Flow Rates**

| Upper Reservoir | | | | |
|---|---|---|---|---|
| Pwf [psi] | q From Equation [bbl/d] | Volume Flow Rate [ft/s] | q From Model [bbl/d] | Percentage Difference [%] |
| 0 | 783.02 | 0.0277 | 426.40 | 45.5441 |
| 500 | 664.38 | 0.0247 | 380.48 | 42.7313 |
| 1000 | 545.74 | 0.0215 | 331.10 | 39.3299 |
| 1500 | 427.10 | 0.0180 | 276.78 | 35.1958 |
| 2000 | 308.46 | 0.0141 | 216.23 | 29.8998 |
| 2500 | 189.82 | 0.0095 | 146.92 | 22.6004 |
| 3000 | 71.18 | 0.0041 | 63.03 | 11.4529 |

**Table 5.16 3.5" Case 4 Flow Rates**

#### *5.2.3.2 Pressure Characteristics*

Figure 5.11 shows the pressure drawdown for the base case and the pressure drawdown on the reservoirs with a flowing bottom hole pressure of 1500 psi for each case is shown in Figure 5.12. These pressure drawdowns show not much change from the base model for the case 1 and case 2. Case 3 is where the pressures can start to be seen changing in the annular and near wellbore regions. Case 4 is where the larger pressure changes can be seen with much higher pressures in the annular area and the higher pressures extending into the reservoir further than any other case.

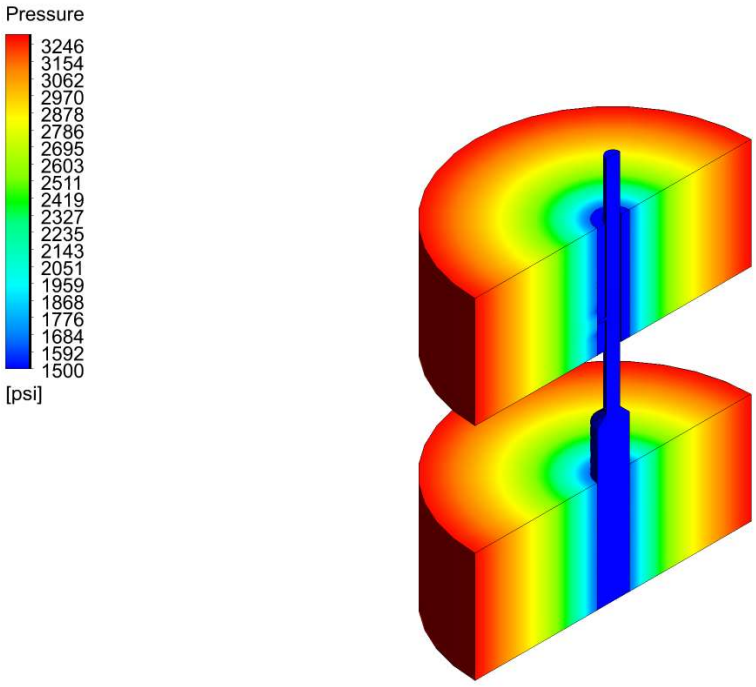


**Figure 5.11 2.875" Model Base Case Pressure Drawdown**

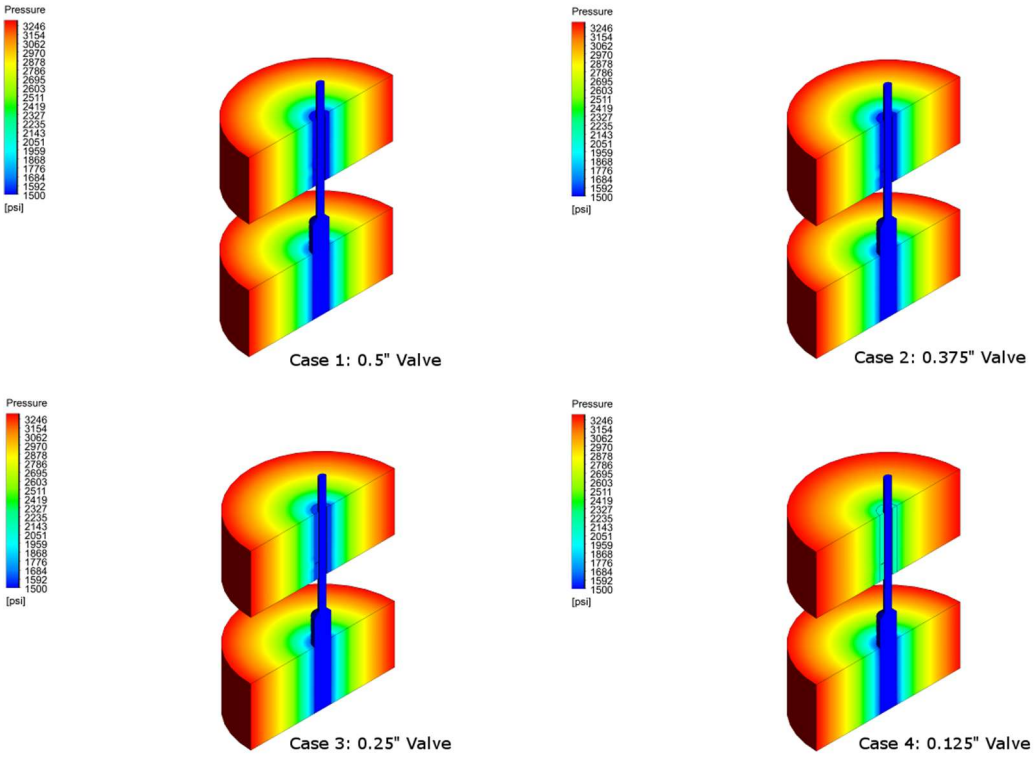


**Figure 5.12 Pressure Drawdowns for Each Case**

Table 5.17 shows the pressures for each case at a distance of 0, 0.5, 1.0, 1.5, 2.0, and 2.5 feet from the wellbore. These pressures show that case 4 is the only one that significantly affects the pressure at the boundary of the reservoir. Each of the other cases shows similar pressures. At the 1.5 foot step case 3 starts to show a higher pressure in the reservoir than case 1 and case 2, and case 4 shows a much higher pressure than any of the others. In the annular area, 0.5 feet from the center of the wellbore, it is shown that cse 3 and case 4 show a higher pressure than the lower cases again with both case 1 and 2 a pressure relatively close to the base case pressure. These pressures correspond with the reduction in pressure that can be seen in the flow rate data. The pressures at each point compare well with the pressures in the 2.875 inch model with the only difference being in case 3 in the near wellbore region showing higher pressures in the 3.5 inch model possibly due to the smaller size of the annulus.

| Upper Reservoir | | | | | |
|---|---|---|---|---|---|
| Distance From Center of Wellbore [ft] | Base Model Pressure [psi] | Case 1 Pressure [psi] | Case 2 Pressure [psi] | Case 3 Pressure [psi] | Case 4 Pressure [psi] |
| 0.0 | 1500 | 1500 | 1500 | 1500 | 1500 |
| 0.5 | 1990 | 1983 | 2004 | 2043 | 2399 |
| 1.0 | 2502 | 2505 | 2508 | 2541 | 2783 |
| 1.5 | 2869 | 2870 | 2872 | 2890 | 3021 |
| 2.0 | 3124 | 3125 | 3125 | 3133 | 3186 |
| 2.5 | 3277 | 3277 | 3277 | 3278 | 3285 |

**Table 5.17 Pressure at Distance for Each Case**

### *5.2.3.3 Velocity Characteristics*

Figure 5.13 shows the velocity characteristics for the base model showing the hghest velocities being through the valve as would be expected.

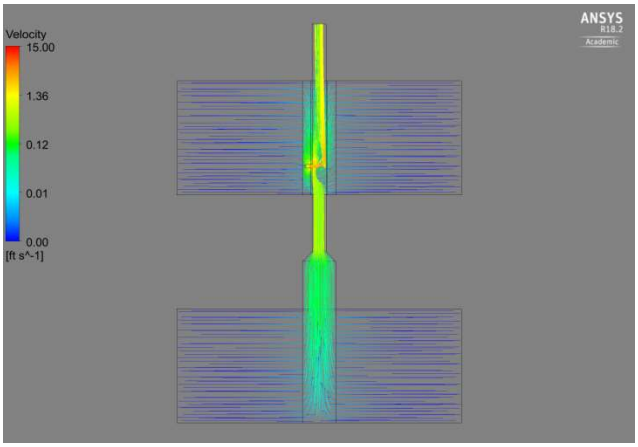


**Figure 5.13 Velocity Streamlines for 3.5" Base Case**

This case again shows the velocity higher in the tubing than in the casing. Comparing this model to the 2.875 inch model shows similar flowrates in the tubing. Figure 5.14 shows the velocity profiles for each of the cases.

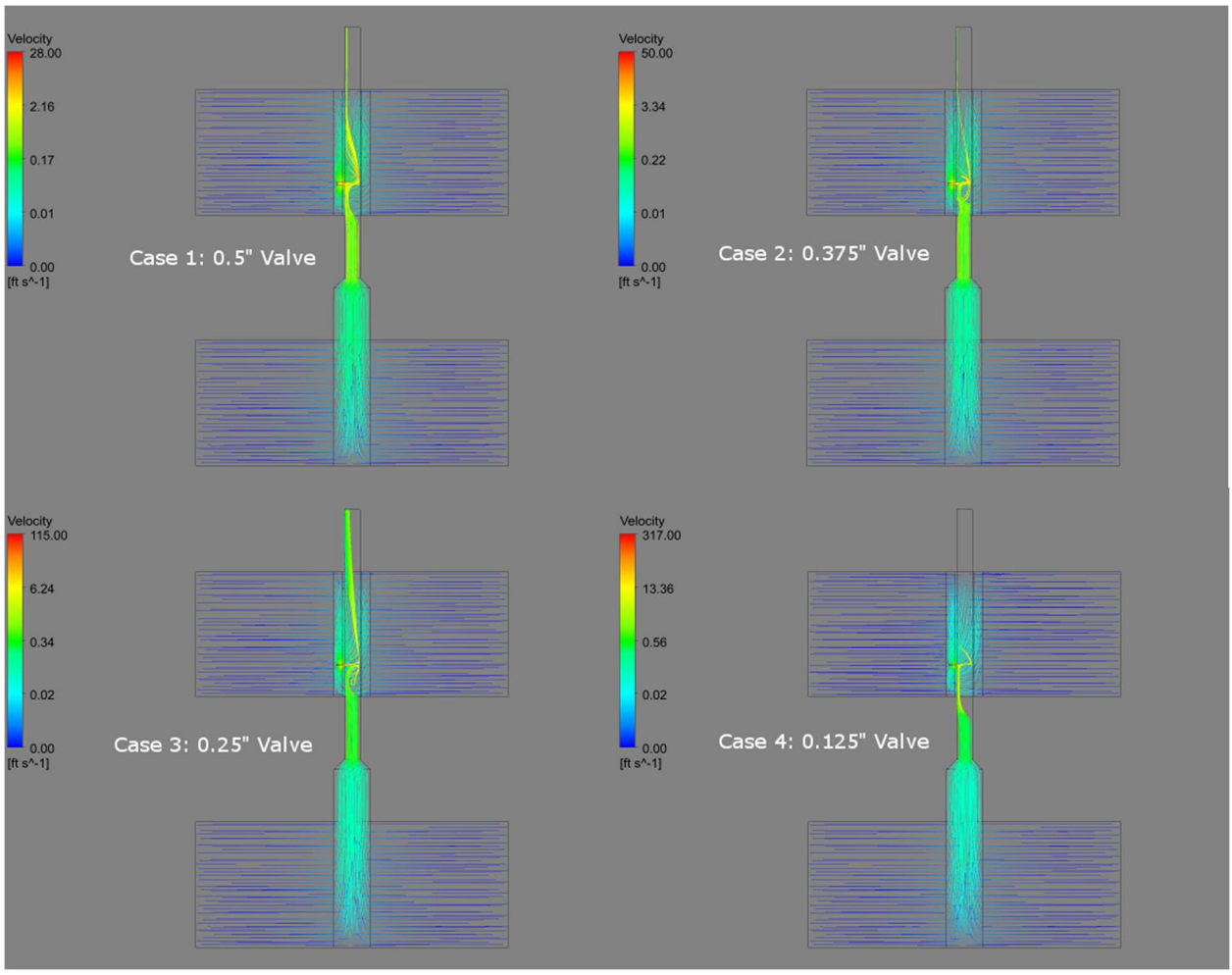


**Figure 5.14 3.5" Model Velocity Profiles for Each Case**

The velocity profiles for each case again show higher velocities as the valve get smaller. This is due to having to move the same amount of fluid through a progressively smaller opening. These profiles also compare well with the 2.875 in model profiles with each case having approximately the same maximum velocity through the valve. Again with the valve in case 4 being small there is the concern for erosion of the valve or the casing due to the higher velocity fluid. It is also important to remember that if the reservoir is known for producing wax, asphaltenes, or sand then this smaller valve has a higher change or clogging than does a larger valve.

### 5.2.4 Well 3: 4.5 inch Model

#### *5.2.4.1 Flow Rate Characteristics*

The final model to be run for the valve scenario was the 4.5 inch tubing model. Table 5.18 shows the flow rates for the lower reservoir. These flow rates again show no reduction in the flow from the lower reservoir due to the introduction of the tubing string and similar to the previous two models each of these cases show a 0.3% or less difference from the base model.

| Lower Reservoir | | | | | |
|---|---|---|---|---|---|
| Pwf [psi] | Base Model Percentage Difference [%] | Case 1 Percentage Difference [%] | Case 2 Percentage Difference [%] | Case 3 Percentage Difference [%] | Case 4 Percentage Diference [%] |
| 0 | 0.6072 | 0.7520 | 0.5576 | 0.4552 | 0.6380 |
| 500 | 0.7493 | 0.6594 | 0.7628 | 0.6690 | 0.6431 |
| 1000 | 0.5824 | 0.6651 | 0.5244 | 0.6498 | 0.5911 |
| 1500 | 0.6896 | 0.6318 | 0.4704 | 0.7233 | 0.7988 |
| 2000 | 0.6495 | 0.6295 | 0.6047 | 0.7136 | 0.8459 |
| 2500 | 0.6151 | 0.6381 | 0.5347 | 0.7016 | 0.5610 |
| 3000 | 0.5722 | 0.6529 | 0.5741 | 0.6712 | 0.6950 |

**Table 5.18 4.5" Model Lower Reservoir Comparison**

The flow rates for the upper reservoir are shown in Figure 5.15. These flow rates show that case 1 and case 2 are similar to the base case as was in both of the previous models. Case 3 is again the first case to show a difference from the base with case 4 showing the largest amount of difference as was also observed in the previous two models.

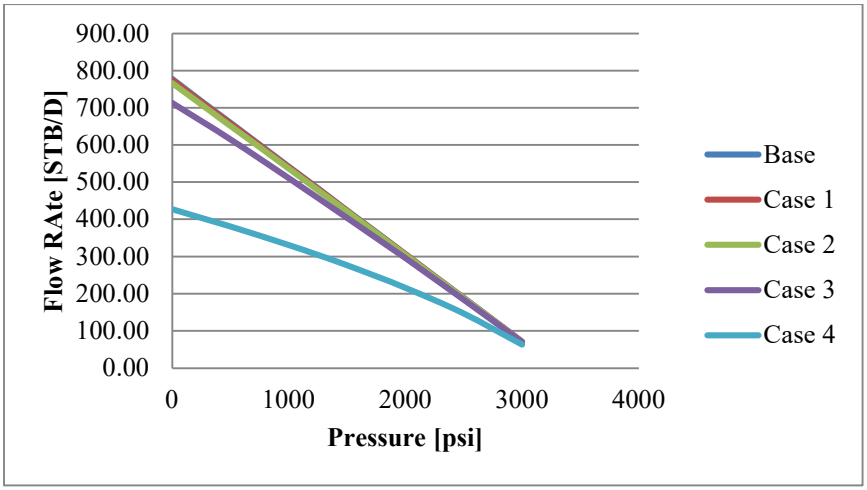


**Figure 5.15 4.5" Model Upper Reservoir Flow Rates**

Table 5.19 and Table 5.20 show the calculated flow rates from case 1 and case 2 respectively. Both of these cases show a slight decrease in production at a flowing bottom hole pressure of zero with case 2 showing a larger decrease but only 2%. Both cases show little to no decrease over the base case for the expected pressure of 1500 psi. These two cases compare with the two previous models case 1 and case 2.

| Upper Reservoir | | | | |
|---|---|---|---|---|
| Pwf [psi] | q From Equation [bbl/d] | Volume Flow Rate [ft/s] | q From Model [bbl/d] | Percentage Diffeernce [%] |
| 0 | 783.02 | 0.0503 | 774.43 | 1.0974 |
| 500 | 664.38 | 0.0427 | 657.16 | 1.0867 |
| 1000 | 545.74 | 0.0351 | 540.36 | 0.9870 |
| 1500 | 427.10 | 0.0275 | 423.28 | 0.8942 |
| 2000 | 308.46 | 0.0199 | 305.82 | 0.8562 |
| 2500 | 189.82 | 0.0122 | 188.41 | 0.7424 |
| 3000 | 71.18 | 0.0046 | 70.69 | 0.6900 |

**Table 5.19 4.5" Case 1 Upper Flow Rates**

| Upper Reservoir | | | | |
|---|---|---|---|---|
| Pwf [psi] | q From Equation [bbl/d] | Volume Flow Rate [ft/s] | q From Model [bbl/d] | Percentage Diffeernce [%] |
| 0 | 783.02 | 0.0498 | 766.85 | 2.0648 |
| 500 | 664.38 | 0.0423 | 651.27 | 1.9741 |
| 1000 | 545.74 | 0.0349 | 536.79 | 1.6406 |
| 1500 | 427.10 | 0.0274 | 421.00 | 1.4296 |
| 2000 | 308.46 | 0.0198 | 304.70 | 1.2185 |
| 2500 | 189.82 | 0.0122 | 187.90 | 1.0145 |
| 3000 | 71.18 | 0.0046 | 70.64 | 0.7705 |

**Table 5.20 4.5" Case 2 Upper Flow Rates**

Table 5.21 and Table 5.22 show the flow rates from the upper reservoir in case 3 and case 4 respectively. Both of these cases show a decrease in production at absolute open flow similar to what was shown in the previous two models. For the expected pressure of 1500 psi a decrease of 5.5% was shown in case 3 and a decrease of 35.2% were seen. These values are similar to the values shown in the previous two models. From this information it can be assumed that the tubing size plays little to no role in the production rates from the upper reservoir. It is possible that at higher rates this would be a factor.

| Upper Reservoir | | | | |
|---|---|---|---|---|
| Pwf [psi] | q From Equation [bbl/d] | Volume Flow Rate [ft/s] | q From Model [bbl/d] | Percentage Diffeernce [%] |
| 0 | 783.02 | 0.0463 | 713.14 | 8.9245 |
| 500 | 664.38 | 0.0400 | 615.39 | 7.3740 |
| 1000 | 545.74 | 0.0332 | 511.23 | 6.3233 |
| 1500 | 427.10 | 0.0262 | 403.87 | 5.4386 |
| 2000 | 308.46 | 0.0192 | 295.47 | 4.2111 |
| 2500 | 189.82 | 0.0120 | 183.92 | 3.1076 |
| 3000 | 71.18 | 0.0046 | 70.15 | 1.4583 |

**Table 5.21 4.5" Case 3 Upper Flow Rates**

| Upper Reservoir | | | | |
|---|---|---|---|---|
| Pwf [psi] | q From Equation [bbl/d] | Volume Flow Rate [ft/s] | q From Model [bbl/d] | Percentage Diffeernce [%] |
| 0 | 783.02 | 0.0278 | 427.02 | 45.4652 |
| 500 | 664.38 | 0.0247 | 380.61 | 42.7127 |
| 1000 | 545.74 | 0.0215 | 330.76 | 39.3927 |
| 1500 | 427.10 | 0.0180 | 276.44 | 35.2765 |
| 2000 | 308.46 | 0.0140 | 216.10 | 29.9418 |
| 2500 | 189.82 | 0.0095 | 146.77 | 22.6782 |
| 3000 | 71.18 | 0.0041 | 62.99 | 11.5171 |

**Table 5.22 4.5" Case 4 Upper Flow Rates**

#### *5.2.4.2 Pressure Characteristics*

In Figure 5.16 the pressure drawdown is shown for the base case and in Figure 5.17 the pressure drawdown for each case is shown at a flowing bottom hole pressure of 1500 psi. The pressure drawdowns for case 1 and case 2 show little difference. These drawdowns match the same cases in the previous two models. Case 3 starts to show a difference in the annular and near reservoir area. These pressures correspond with a decrease in production as was shown in the previous section. Case 4 shows a larger pressure increase in the annular and near reservoir region as would be expected due to the decrease in production. In this well model a difference can be seen in the pressure around the valve area where a higher pressure is observed directly adjacent to the valve. This higher pressure is likely caused by the fluid in the annulus entering the valve and causing the fluid in the reservoir to no have a path into the

wellbore. This phenomenon was not as prevalent in the 2.875 or 3.5 inch model but can be seen with a close examination of the pressure drawdown images.

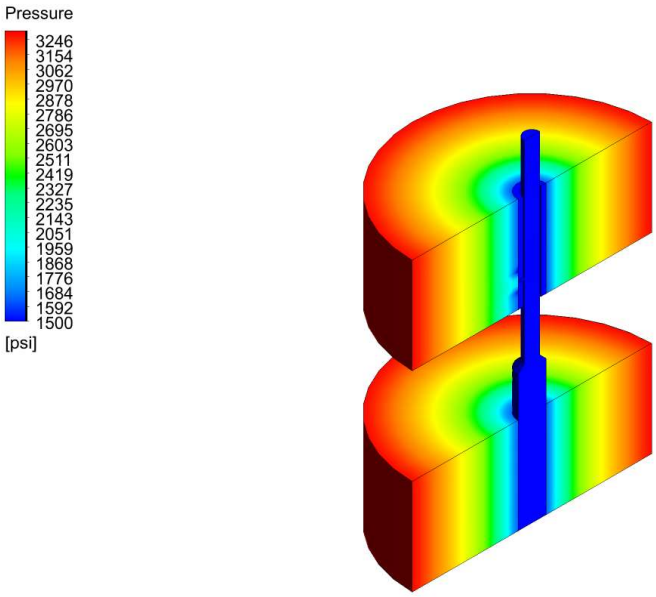


**Figure 5.16 4.5" Model Base Case Pressure Drawdown**

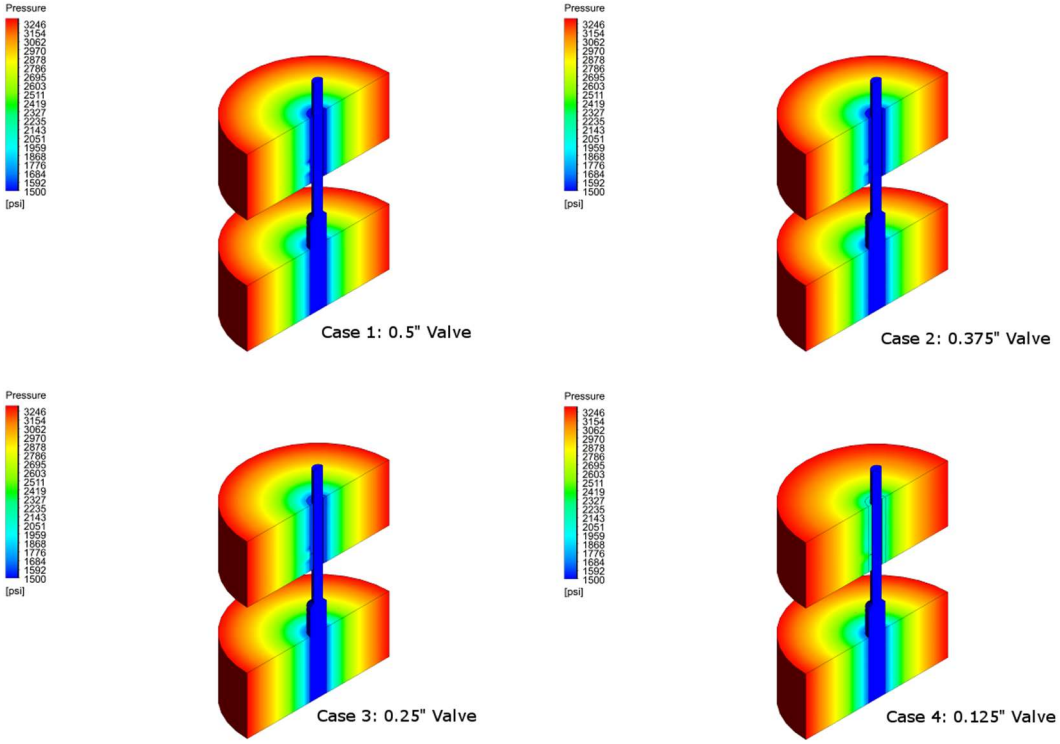


**Figure 5.17 4.5" Model Pressure Drawdown**

The pressures from the drawdown can be seen in Table 5.23 where distance of 0, 0.5, 1.0, 1.5, 2.0, and 2.5 feet from the reservoir are shown for each case. For case 1 and case 2 there is little change in the pressure in the reservoir or the annular area. For case 3 there is a higher pressure in the near reservoir region and in the annular area due to the decrease in production as was shown in Figure 5.17 for the drawdown. Case 4 shows a much larger increase in pressure over the base case as is similar to both the 2.875 and 3.5 inch models performed before. Similar to the 3.5 inch model the annular area starts to build more pressure for both case 2 and case 3 due to the smaller annular area present to store fluid before it goes through the valve.

| Upper Reservoir | | | | | |
|---|---|---|---|---|---|
| Distance From Center of Wellbore [ft] | Base Model Pressure [psi] | Case 1 Pressure [psi] | Case 2 Pressure [psi] | Case 3 Pressure [psi] | Case 4 Pressure [psi] |
| 0.0 | 1500 | 1500 | 1500 | 1500 | 1500 |
| 0.5 | 2138 | 2170 | 2079 | 2230 | 2578 |
| 1.0 | 2504 | 2506 | 2506 | 2542 | 2776 |
| 1.5 | 2870 | 2871 | 2871 | 2890 | 3016 |
| 2.0 | 3125 | 3125 | 3125 | 3133 | 3184 |
| 2.5 | 3277 | 3277 | 3277 | 3278 | 3285 |

**Table 5.23 4.5" Model Pressures at a Distance**

#### *5.2.4.3 Velocity Characteristics*

The velocity streamlines for the base case are shown in Figure 5.18. Similar to the previous two models this shows a higher velocity going through the valve than in any other location. Also the velocity increases as the fluid leaves the casing and enters the tubing. Much like the 3.5 inch model this difference is no perceptible difference in the velocities in the streamline plot.

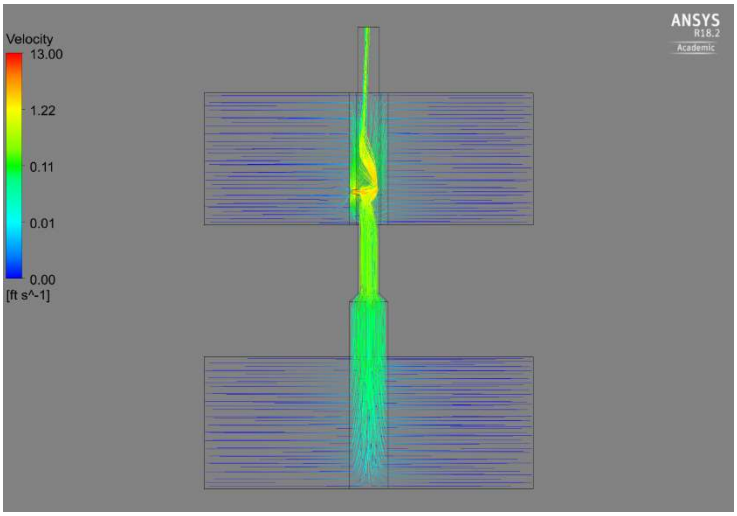


**Figure 5.18 4.5" Base Case Velocity Streamlines**

Equation 5.12 gives the way to calculate the flow rate in ft/s based on the flow rate in bbl/d for a given size tubing with q in $ft^3/s$ and d in ft. Using this equation the flow rate in the tubing was calculated for each of the models and is shown in Table 5.24.

$$v = \frac{4q}{\pi d^2} \qquad [5.12]$$

The velocity in the tubing is much lower than the velocity in the valve. These velocities are similar for each tubing size with the 2.875 in tubing having the highest velocity and the 4.5 inch tubing the lowest.

| Flow Rate [bbl/d] | Flow Rate [ft3/d] | Velocity in 2.875" Tubing [ft/s] | Velocity in 3.5" Tubing [ft/s] | Velocity in 4.5" Tubing [ft/s] |
|---|---|---|---|---|
| 696.02 | 0.045 | 0.240 | 0.197 | 0.154 |
| 590.56 | 0.038 | 0.204 | 0.168 | 0.130 |
| 485.10 | 0.032 | 0.168 | 0.138 | 0.107 |
| 379.65 | 0.025 | 0.131 | 0.108 | 0.084 |
| 274.19 | 0.018 | 0.095 | 0.078 | 0.061 |
| 168.73 | 0.011 | 0.058 | 0.048 | 0.037 |
| 63.27 | 0.004 | 0.022 | 0.018 | 0.014 |

**Table 5.24 Velocities in Tubing Below Valve**

Figure 5.19 shows the velocity profiles for each of the cases. The velocity through the valve increases as the valve decreases in size, as was shown in the previous two models. The velocities shown are similar to the velocities in the 2.875 and 3.5 inch model as well. This leads to the conclusion that the valve is the controlling factor on the velocity in the system.

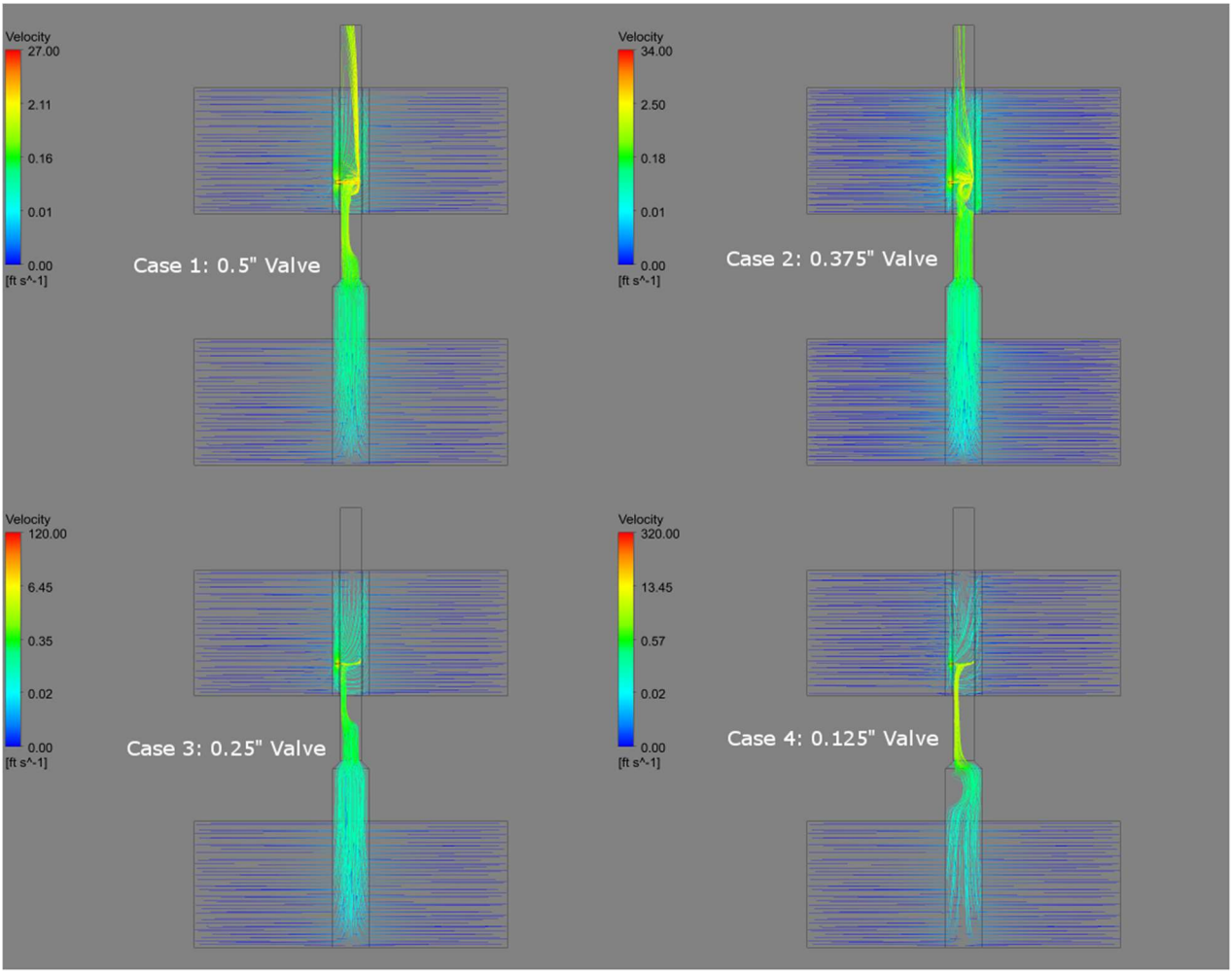


**Figure 5.19 4.5" Velocity Streamlines**

## 5.3 Sliding Sleeve Model

### 5.3.1 Flow Rate Characteristics

The sliding sleeve model was designed in much the same way as the mandrel model with the major difference between the models being that there were 4 connecting points from the tubing into the annular area to show the four different flow paths available in the sleeve. This model is much larger, in terms of computational power, than the mandrel model and borders on the limits of the academic version of the ANSYS software as well as the limits of the modeling computer that was available for use for this reason and because of the results only the one model was run. For these reasons the sleeve model was only run with one port size being 0.125 inches and 3.5 inch tubing. Figure 5.20 shows a cross section of the sliding sleeve model where ports 180 degrees from each other are visible.

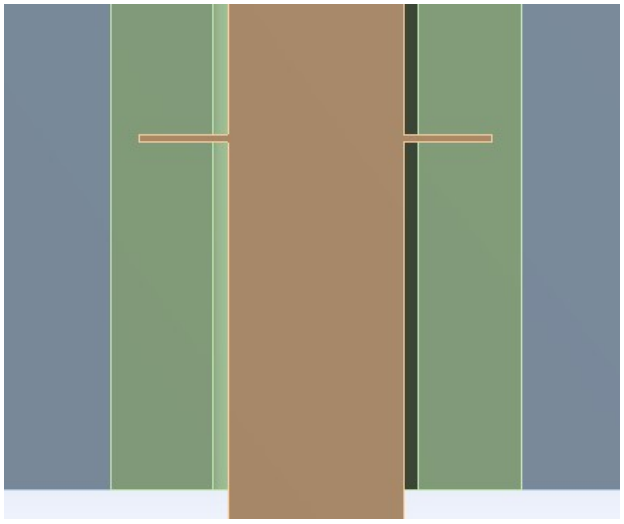

**Figure 5.20 Cross-Sectional View of Sleeve Model**

The lower reservoir again flowed unencumbered through the 3.5 inch tubing in the model as with all of the previous mandrel models and Table 5.25 shows this data.

| Lower Reservoir | | |
|---|---|---|
| Pwf [psi] | Base Model Percentage Difference [%] | Sleeve Model Percentage Difference [%] |
| 0 | 0.7224 | 0.4268 |
| 500 | 0.6578 | 0.5453 |
| 1000 | 0.6280 | 0.5700 |
| 1500 | 0.6349 | 0.5315 |
| 2000 | 0.6446 | 0.5131 |
| 2500 | 0.6406 | 0.5413 |
| 3000 | 0.6498 | 0.5323 |

**Table 5.25 Sliding Sleeve Model Lower Reservoir Flow Rates**

The upper reservoir flow data shows that reduction in production was similar to the 0.25 inch valve for each of the mandrel models. Table 5.26 shows the flow data from the upper reservoir compared to the base 3.5 inch mandrel model and case 3 of the 3.5 inch mandrel model. In order for this model to start to show a reduction in flow similar to the 0.125 inch mandrel model the valve would have to be of a size that it would to easily clog with wax, asphaltenes, or sand from the reservoir and would be of little use and cause intervention costs to skyrocket for the well.

| Upper Reservoir | | | | |
|---|---|---|---|---|
| Pwf [psi] | q From Equation [bbl/d] | Volume Flow Rate [ft/s] | q From Model [bbl/d] | Percentage Diffeernce [%] |
| 0 | 783.02 | 0.0470 | 723.89 | 7.5512 |
| 500 | 664.38 | 0.0403 | 620.00 | 6.6795 |
| 1000 | 545.74 | 0.0335 | 515.09 | 5.6170 |
| 1500 | 427.10 | 0.0265 | 407.88 | 4.5016 |
| 2000 | 308.46 | 0.0194 | 297.98 | 3.3971 |
| 2500 | 189.82 | 0.0121 | 185.62 | 2.2149 |
| 3000 | 71.18 | 0.0046 | 70.42 | 1.0796 |

**Table 5.26 Sliding Sleeve Model Upper Reservoir Flow Rates**

### 5.3.2 Pressure Characteristics

The pressure characteristics for the sliding sleeve mode are shown in Figure 5.21.

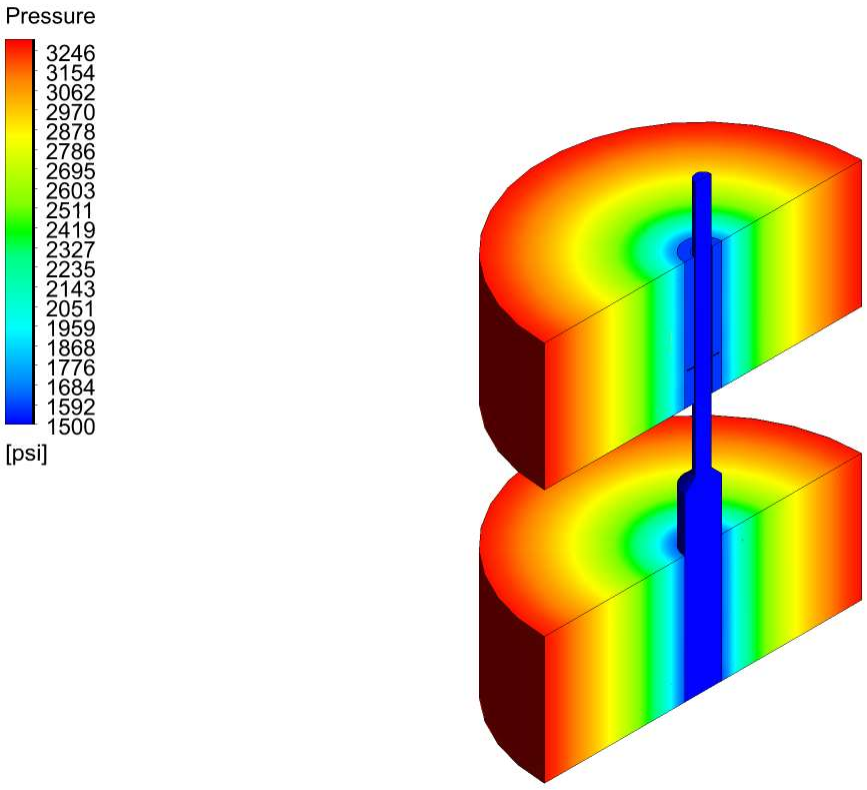


**Figure 5.21 Sliding Sleeve Pressure Drawdown**

These pressures are similar to the ones seen in the 0.25 inch valve case of each of the previous mandrel models as is shown in Table 5.27. The pressure diagram does not show the higher pressure in the

reservoir near the connection from the annulus and the tubing as was seen in the 3.5 inch model for the mandrel setup. This is most likely because there are more entry points for the fluid into the tubing from the reservoir so there is not as much fluid backed up from the reservoir.

| Upper Reservoir | | | |
|---|---|---|---|
| Distance From Center of Wellbore [ft] | 3.5" Mandrel Base Model Pressure [psi] | 3.5" Mandrel Case 3 Model Pressure [psi] | Sleeve Model Pressure [psi] |
| 0.0 | 1500 | 1500 | 1500 |
| 0.5 | 1990 | 2043 | 2102 |
| 1.0 | 2502 | 2541 | 2633 |
| 1.5 | 2869 | 2890 | 2900 |
| 2.0 | 3124 | 3133 | 3101 |
| 2.5 | 3277 | 3278 | 3265 |

**Table 5.27 Sliding Sleeve Model Pressure Comparisons**

The pressures mimic more of the 0.25 inch valve than they do the base case for the 3.5 inch mandrel model. This would be expected as the flow rates also are more in line with the same case from the previous run mandrel models. The curious part of this model is that the pressures further out in the reservoir are showing lower in the sleeve model than in the mandrel model. This is possibly due to modeling error but was replicated several times. It is possible that with more flow paths open for the fluid the reservoir is able to more evenly drain. The points chosen for the pressure data are directly in line with the valve in the mandrel model. In this model the fluid has to come from all sides of the reservoir to enter the tubing at one point. This could cause a backup in the reservoir and result in higher pressures near the boundary. With more flow paths there is less fluid near the entry point on the left hand side of the model so less chance for the fluid to be stored in the reservoir and thus lower pressures.

### 5.3.3 Velocity Characteristics

Figure 5.22 shows the velocity streamline profile for the sliding sleeve model. The velocity streamlines show the same rates as the 0.25 inch valve models do for the previous mandrel models with the only difference being that flow is entering the tubing from more than one point. Figure 5.23 shows a top view of the reservoir for the sliding sleeve model and case 3 of the 3.5 inch mandrel model.

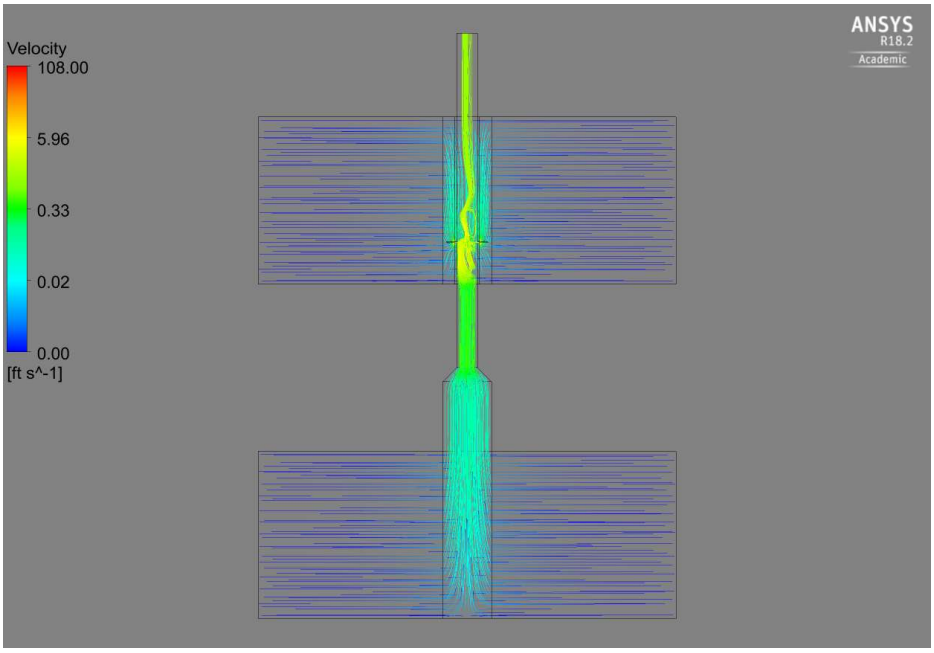


**Figure 5.22 Sliding Sleeve Model Velocity Streamlines**

This comparison shows how the fluid has to flow around the annular area into the single valve in the 3.5 inch mandrel model versus having multiple flow paths from the sliding sleeve model. With the four entry points in the sliding sleeve model cause the fluid to have slightly less velocity overall than in the single entry point from the 0.25 inch valve. Also with an entry point directly opposite from each of the entry points less erosion will be seen on the tubing as the fluid will not have a chance to reach the opposite wall of the tubing as can also be seen in Figure 5.23. This four entry point setup would be a better choice than a single valve setup if only a small reduction in flow was required. Also since the reduction in flow is contingent on the fluid flow a reservoir with much higher flow than the 380 bbl/d that is seen from the model will result in a larger reduction of flow.

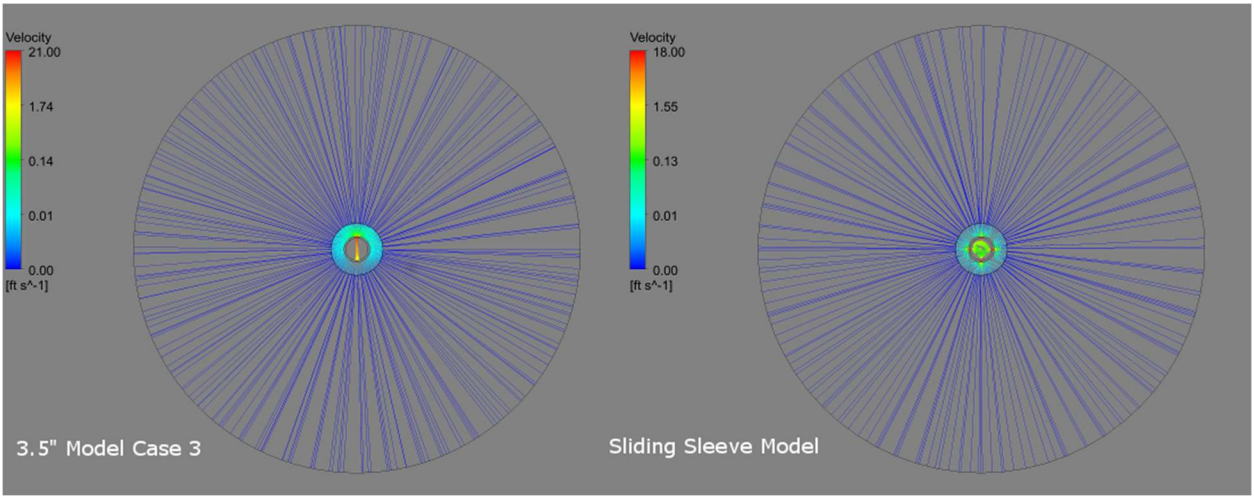


**Figure 5.23 3.5" Case 3 Vs. Sliding Sleeve Velocity Streamlines**

# 6 Chapter Six: Conclusions and Recommendations

## 6.1 Conclusions

Two different scenarios, production through a mandrel valve or a sliding sleeve, were evaluated for flow characteristics. These models were compared to each other to see which would be best at reducing flow from the upper reservoir and how they would affect flow from the lower reservoir. For the mandrel model three different models were run with the same four cases being run for each model. It was shown that for each case examined the flow was the same regardless of the tubing size indicating that the valve plays the largest role in the flow control from the reservoir. The sliding sleeve model best resembled the 0.25 inch case 3 from each of the mandrel models.

The pressure characteristics were looked at and showed the same for each model and case with the exception being that pressures in the reservoir were higher near the valve the increase in tubing size. This was compared to the sliding sleeve model with four entry points from the annulus into the tubing and this pressure increase was not observed due to the fluid being able to enter the tubing in more areas and not resulting in a backup in the annular area near the valve. The pressures in the sliding sleeve model were also lower at deeper interval in the reservoir because of these increased flow paths.

The velocity streamlines were also observed to see the maximum velocity through the valve and possible erosional effects on the tubing and valve. As the valve was reduced in size the velocity increased as expected but also resulted with fluid hitting the opposite side of the tubing with a higher velocity which over time could result in more erosional effects on the tubing. The sliding sleeve model was observed to have less velocity for the same size valve due to the larger number of flow paths for the fluid to enter the tubing. Also with this model the erosional effects are not as high due to an entry point being directly across for each entry point. This will allow the fluid to buffer itself and not strike the wall of the tubing.

The velocity is important to consider when choosing a valve size as the erosional effects on the valve may result in costly interventions. Another aspect to consider when picking valve size is if the reservoir makes a lot of sand, wax, or asphaltenes. These products can clog the valve again causing costly interventions. The sleeve model again poses a better option in one of these situations as there are more flow path into the wellbore. The downside for a sleeve model is that the sleeve cannot be replaced by a wireline unit and would require a workover rig being brought in to pull the tubing and change the sleeve if it becomes too clogged with debris. A mandrel valve setup is less costly in this aspect as a wireline unit can pull a valve and set a new one in less than a day.

## 6.2 Recommendations for Future Work

- Larger more detailed model to better understand the flow paths in the tubing and annular area. Use of the full version of Fluent so that more than 512,000 nodes can be employed.
- Comparison of model results to actual production data from well with a single-string multi-zone design to determine if the results match real world scenarios.
- More detail in the area of perforations instead of an openhole completion.
- Model of deviated and horizontal wells
- Multi-phased flow model with two phase oil-water, oil-gas, and three phase oil-water-gas flows with higher gas flow or water flow rates from the upper reservoir needing to be choked back more effectively.
- More detailed look at pressure drawdowns for the single fluid entry path on the mandrel valve system to belter examine the pressure phenomena seen with the larger tubing sizes.
- More detailed model in the area of heat transfers from the reservoir to the tubing, how much heat is lost in the valve and does it affect the flowing temperature of the well with respects to waxes and asphaltenes.

# 7 References


Amear, S. A., & Almoayyed, A. R. (1979). *Single-String Multi-Zone Completions In The Bahrain Field*. Paper presented at the SPE Middle East Technical Conference, Manama, Bahrain.

Anderson, J. D. (1995). *Computational Fluid Dynamics The Basics with Application*. New York, NY: McGraw-Hill.

ANSYS. (2013a). *ANSUS Fluent User's Guide* (Release 15.0 ed.).

ANSYS. (2013b). *ANSYS Fluent Theory Guide* (Release 15.0 ed.).

Byrne, M., Alejandra, M., & Chavez, J. J. C. (2009). *Predicting Well Inflow Using Computational Fluid Dynamics -- Close to the Truth?* Paper presented at the SPE European Formation Damage Conference, Scheveninge, The Netherlands.

Byrne, M. T., Jimenez, M. A., Rojas, E. A., & Chavez, J. C. (2010). *Modeling Well Inflow Potential in Three Dimensions Using Computational Fluid Dynamics*. Paper presented at the SPE International Symposium and Exhibition on Formation Damage Control, Lafayette, Louisiana, USA.

Chen, N. H. (1979). An Explicit Equation for Friction Factor in Pipe. *Ind. Eng. Chem. Fundam, 18*(3), 296-297.

Chorin, A. J. (1968). Numerical Solutions of the Navier-Stokes Equations. *Mathmatics of Computation, 22*(104), 745-762.

Craft, B. C., & Hawkins, M. (1991). *Applied Petroleum Reservoir Engineering* (Second ed.).

Darcy, H. (1856). *The Flow of Homogeneous Fluids Through Proous Media*.

Jensen, T. B., Little, L., Melvin, J., Reinbold, E., Jamieson, D., & Shi, W. (2012). *Kuparuk River Unit Field - The First 30 Years*. Paper presented at the SPE Annual Technical Conference and Exhibition, San Antonio, Texas.

Jimenez, M.-A., & Chavez, J. C. (2009). *Understanding the Near-wellbore Phenomena for Hydrauically Fractured wells: A Comprehensive Inflow Performance Numerical Model*. Paper presented at the SPE European Formation Damage Conference, Scheveningen, The Netherlands.

Kaszuba, F. (2004). United States of America Patent No. US 6,763,892 B2.

Li, L. J., Zhang, H., Davis, G. R., & Hamid, S. (2005). *Improving the Closing Characteristics of Subsurface Safety Valve with Combined FEA and CFD Modeling/Numerical Analysis*. Paper presented at the SPE Western Regional Meeting, Irvine, Calafornia, USA.

Longfellow, N., & Green, D. (2014). *Computational Fluid Dynamics for Horizontal Well Plunger Lift System Design*. Paper presented at the SPE Western North American and Rockey Mountain Joint Regional Meeting, Denver, Colorado.

Molina, O. M. (2015). *Application of Computational Fluid Dynamics to Near-Wellbore Modeling of a Gas Well.* (Masters of Science), Louisiana State University,

Rae, C. G. (2013). European Patent Office Patent No. EP 2 631 418 A2.

Reaux, J. (2013). United States of America Patent No. US 8,353,353 B2.

Sun, D., Li, B., Gladkikh, M., Satti, R., & Evens, R. (2013). *Comparison ofSkin Factors for Perforated Completions Calculated With Computational-Fluid-Dynamics Software and the Karakas-Tariq Semianalytical Model*. Paper presented at the SPE European Formation Damage Conference, Noordwijk, The Netherlands.

Tennekes, H., & Lumley, J. L. (1972). *A first Course in Turbulence*.

Theppornprapakorn, V. (2013). *Computational fluid dynamics flow comparison between openhole sleeve and plug-and-perf completion in a hydraulic fractured horizontal well.* (Masters of Science), Missouri University of Science and Technology,

VanEverdingen, A. F., & Hurst, W. (1949). *The Application of the Laplace Transformation to Glow Problems in Reservoirs*. Paper presented at the AIME Annual Meeting, San Francisco, Calafornia, USA.

Versteeg, H. K., & Malalasekera, W. (2007). *An Introduction to Computational Fluid Dynamics The Finite Volume Method* (2nd ed.).

Zhou, Y., & Shah, S. N. (2003). *Fluid Flow in Coild Tubing: CFD Simulation*. Paper presented at the Petroleum Society Canadian International Petroleum Conference, Calgary, Alberta, Canada.